A HYBRID PHYSICS AWARE LEARNING BASED TRANSMISSION LINE RESISTANCE ESTIMATION ALGORITHM FOR DYNAMIC LINE RATING APPLICATION

A Dissertation by

Anton C. Sameepa Hettiarachchige-Don

Master of Science, Wichita State University, 2016

Bachelor of Science, Southeast Missouri State University, 2014

Submitted to the Department of Electrical Engineering and Computer Science
and the faculty of the Graduate School of
Wichita State University
in partial fulfillment of
the requirement for the degree of
Doctor of Philosophy

May 2021

A HYBRID PHYSICS AWARE LEARNING BASED TRANSMISSION LINE RESISTANCE ESTIMATION ALGORITHM FOR DYNAMIC LINE RATING APPLICATION

The following faculty members have examined the final copy of this dissertation for form and content, and recommend that it be accepted in partial fulfillment of the requirement for the degree of Doctor of Philosophy, with a major in Electrical Engineering.

_____
Visvakumar Aravinthan, Committee Chair

_____
Ward Jewell, Committee Member

_____
Chengzong Pang, Committee Member

_____
M. Edwin Sawan, Committee Member

_____
Ehsan Salari, Committee Member

Accepted for the College of Engineering

_____
Steven Skinner, Interim Dean

Accepted for the Graduate School

_____
Coleen Pugh, Dean

DEDICATION

To my parents for their continuous love and encouragement.
And to my loving wife for her unconditional understanding and support

ACKNOWLEDGMENTS

I would like to express my sincere gratitude and heartfelt appreciation for my advisor, Dr. Visvakumar Aravinthan for all the guidance, support and encouragement throughout my graduate years. Over the 7 years I have known and worked with him, he has become a great mentor, not just academically but also personally. Beyond anything else, Dr. Ara has made me rethink what I believed to be expected of me.

I would like to thank my committee member Dr. Ward Jewell, whose previous studies form the starting point for this work. I would also like to thank him for providing me with the necessary data and resources, as well as connecting me to the utility partner in this work. His expertise on this area of study was invaluable. I would also like to thank my committee member and mentor Dr. Edwin Sawan, who was always there to support me throughout this journey. I would like to thank him for sharing with me his wisdom and experience, not just in academia, but also in life. I would also like to extend my gratitude for Dr. Sawan's Maha "Maggie" Sawan Fellowship in memory of his late wife. I was honored to be a recipient of this fellowship during my time as a Doctoral Student.

I would like to thank my committee member Dr. Chengzong Pang for his support, advice, time and for being a part of this committee. I would also like to extend my appreciation towards my committee member Dr. Ehsan Salari for his support in the area of modeling theory and for being a part of this committee.

I would like to thank our utility partner for providing, not just the necessary data, but also their expert advice and recommendations. I would like to thank my peers without whom this journey would not have been possible. Arun-Kaarthick Manoharan, Nimanthi Nandasiri, Suvagata Chakraborty, Rakib Ur Rahman and Sultan Hakmi, thank you for sticking together, through laughter and hardship. Their professional advice, inputs and contributions to this work were numerous but even greater were their friendships and the comradery. I would also like to appreciate the support, guidance and encouragement

given by my dear friends, both in Wichita and elsewhere, who each in their own capacity have helped me to reach this goal.

I would like to thank my loving wife, Dr. Umesha Perera, for her encouragement, understanding, and sacrifice and for staying by my side, through many hardships, all the way from day one.

Lastly, above all else, the deep gratitude I extend towards my parents is beyond words. Thank you for your never-ending support and encouragement. I am confident that my accomplishment here is a worthy return for all the trust that they placed upon me.

ABSTRACT

The worldwide push towards a more intelligent, connected and reliable electric power delivery system has led to the propagation of a wide range of new technologies and ideas within the power grid infrastructure. Thus, the power grid is becoming more adaptable to changes and more reliable under distress. However, these benefits are only possible with vastly improved observability in the system. The traditional methods and technologies for grid monitoring were simply too slow and newer, faster and more accurate monitoring technologies became essential over the turn of the century.

With the advancement of micro processing and communication technologies at an incredibly fast pace, this became possible in the form of smart monitoring devices. These devices include Intelligent Electronic Devices (IEDs), smart meters for homes and, at the transmission level, the use of Synchrophasor Measurement Units (PMUs). Over the past decade, transmission utilities were quick to adopt these PMU networks and they are now common among most major utilities. Compared to traditional monitoring systems, PMUs provide information at a much higher resolution and have the advantage of being time synchronized. The benefits of these networks are numerous, but they are not without certain drawbacks.

PMU devices only report some basic system parameters from the field. While these are useful on their own, it is possible to use this data, in combination with other information, to extrapolate additional parameters about the grid. However, in this process, inherent errors present in PMU estimated data become an issue and renders the results of this extrapolated information unusable. In this work, of particular focus from these additional parameters is transmission line resistance. The fundamental cause of error will be investigated, and this knowledge will be applied to create a correction algorithm to output corrected transmission line resistance estimates that are more useful to utilities for a range of auxiliary applications such as dynamic line rating, determination of line sag, and conductor temperature estimation. This advancement would allow utilities to compound the economic benefits of their investment in PMU networks.

TABLE OF CONTENTS

TABLE OF CONTENTS (continued)

LIST OF TABLES

LIST OF FIGURES

LIST OF FIGURES (continued)

LIST OF FIGURES (continued)

LIST OF ABBREVIATIONS

AC	Alternating Current
ACSR	Aluminum Conductor Steel Reinforced
ADC	Analog to Digital Convertor
AEP	American Electric Power Service Corporation
ANN	Artificial Neural Network
BPA	Bonneville Power Administration
CAPE	Computer-Aided Protection Engineering
CCVT	Coupling Capacitor Voltage Transformer
CT	Current Transformer
DLR	Dynamic Line Rating
EIA	Energy Information Administration
GB	Giga Byte
GOES	Geostationary Operational Environmental Satellite
GPS	Global Positioning System
Hz	Hertz
IED	Intelligent Electronic Device
IEEE	Institute of Electrical and Electronics Engineers
ISO	Independent System Operator
KKT	Karush-Kuhn-Tucker
LSQ	Least Squares method
MPME	Maximum Percentage Magnitude Error
NASPI	North American SynchroPhasor Initiative

NERC	North American Electric Reliability Corporation
NYPA	New York Power Authority
PLO	Phase-Locked Oscillator
PMU	Synchrophasor Measurement Unit
PT	Potential Transformer
RDM	Recursive Decoupled Minimization
RMS	Root Mean Square
SCADA	Supervisory Control And Data Acquisition
SCDR	Symmetrical Component Distance Relay
SGIG	Smart Grid Investment Grant Program
SOC	Second Of Century
TVE	Total Vector Error
UTC	Universal Coordinated Time

CHAPTER 1

INTRODUCTION

Over the past several decades, the world's electric power grids have undergone significant changes. According to U.S. Energy Information Administration (EIA) statistics, the worlds electrical energy needs have increased significantly and this trend has gone in conjunction with the widescale implementation of renewable energy sources. These trends are showcased in Figure 1. Environmental concerns, positive public perception and the overall economic and political viability of such projects have massively driven up the implementation of large-scale renewable resources in favor of traditional energy sources.

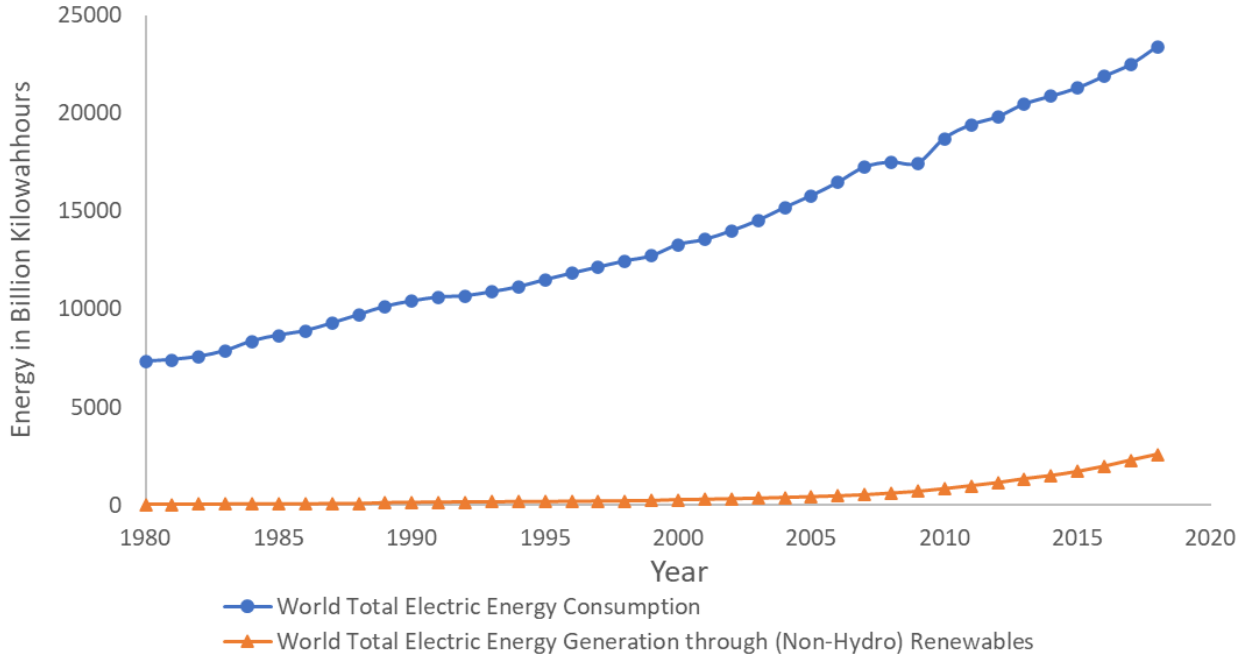

Figure 1. Worldwide annual electric energy consumption and (non-hydro) renewable energy generation [1].

Renewable sources, however, bring with them a number of challenges pertaining to their integration into the existing power system. Firstly, renewable sources tend to be more geographically distributed than traditional sources. Thus, instead of a single large power plant that

supplies the bulk of the region's power, the same generation capacity could be distributed among several wind or solar generation farms at varied locations throughout a state or country. Secondly, in comparison to the largely predictable power output from a traditional coal or natural gas plant, the output of renewable sources could be highly intermittent. Thus, simple events, such as a sudden cloud cover over a solar farm or a sudden drop in wind speed across a wind farm, could result in a significant drop in power output from the source. For these reasons, the integration of renewable sources make the system highly dynamic and difficult to predict.

Due to this, the modern power system requires high levels of real-time observability and decision making. This capability is largely enabled at the transmission level with the implementation and use of Synchrophasor Measurement Units (PMUs) as discussed in detail in Chapter 2.

In contrast to a traditional centralized system where the bulk power from a large power plant could be carried out with a few high-capacity lines, in a distributed network, the nature of renewable sources means that in order to make the maximum and most efficient use of their output, it is necessary to know the current carrying capacity of the many transmission lines connected to the sources as well as those within the network. This is the study of Dynamic Line Rating (DLR).

1.1 Dynamic Line Rating and Line Resistance

The line rating is the current carrying capacity, also called the ampacity, of a transmission line. It is a function of many factors, and most significantly, the resistance of the conductor. Other factors include ambient temperature, wind direction and speed and solar radiation. Historically, the line rating limits have been static values calculated from physical properties of the line, the conductor material and the environmental conditions.

This approach did well when the power system was far less dynamic. However, in the modern grid, there are several disadvantages with this approach.

Firstly, in order to maintain a margin of safety under adverse weather conditions, the limits are set conservatively. However, this means that under ideal conditions, the transmission lines are not utilized effectively. A study on the use of conductor temperature sensors and line sag monitoring devices shows the benefits of dynamic line ratings in contrast to static ratings [2].

As shown in Figure 2, due the conservative nature of the static rating, a large portion of usable current carrying capacity goes unutilized. At the same time, under certain conditions, it is also possible for the actual current carrying capacity to dip below the static levels and thus putting the lines at risk of overheating.

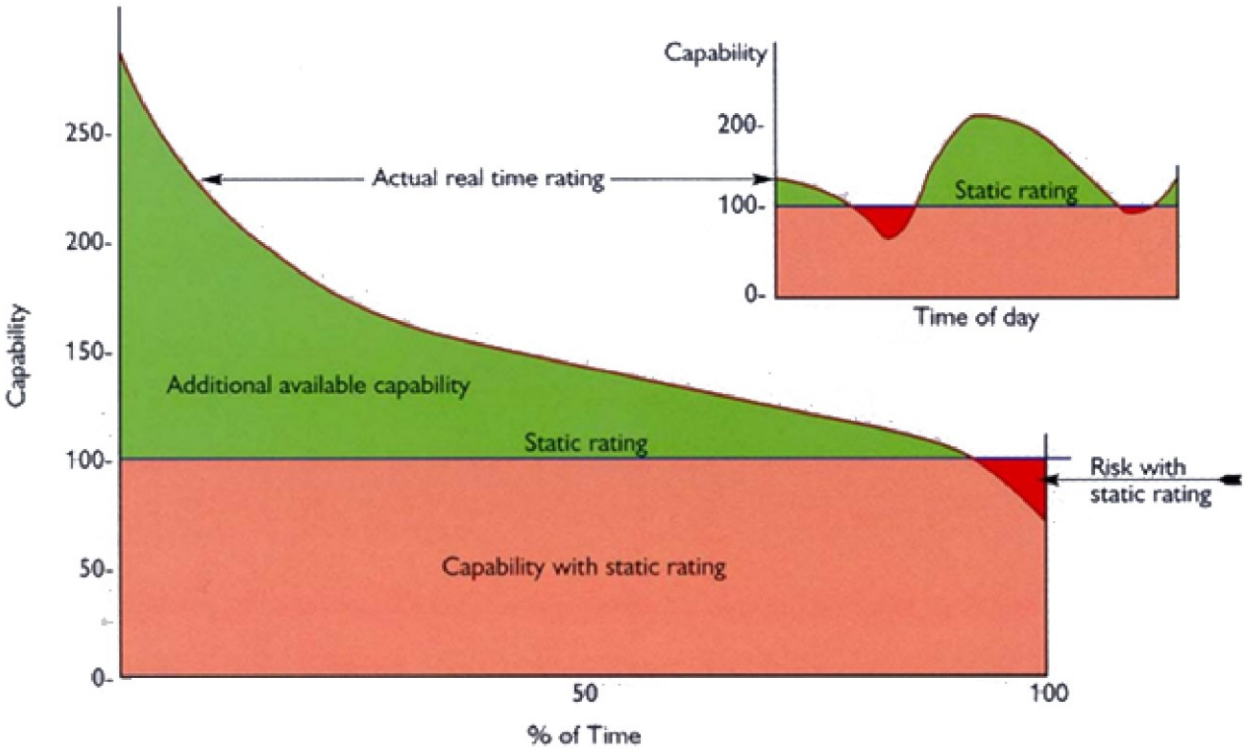

Figure 2. Inefficiency of static line ratings [2].

To elaborate this effect, a study conducted on a 20-mile Aluminum Conductor Steel

Reinforced (ACSR) transmission line is detailed in Table 1. With a static line rating of 787A at daytime with an ambient temperature of 40 degrees Celsius and no wind, the line was tested under various environmental condition changes to determine its actual ampacity under those conditions [3].

TABLE 1

CHANGES TO AMPACITY WITH CHANGES IN ENVIROMENTAL CONDITIONS [3]

Environmental Conditions	**Change in Ampacity**
Ambient Temperature	
2°C fluctuation in ambient	+/- 2% capacity
10°C drop in ambient	+ 11% capacity
Solar Radiation	
Cloud shadowing	+/- a few percent
Middle of night	+ 18% capacity
Wind Increase of 1 m/s	
45° angle	+ 35% capacity
95° angle	+ 44% capacity

The factors detailed above and the associated variations in ampacity can be calculated mathematically with a fair degree of accuracy. Apart from these external factors, the variation in ampacity due to heating through resistance is a major factor in the determination of dynamic line rating. However, due to the complications arising from the many additional factors involved, this change is often not determined mathematically. Instead, physical testing is used to determine the resistance values of conductors at 2 or more set current flow values, as a ratio of line capacity, and

this information is provided in the datasheets [4]. These resistance values are then used to calculate the line rating.

Therefore, the ability to dynamically determine a transmission line resistance values instead of resorting to predetermined values would be an important step towards the ability to obtain more accurate dynamic line ratings [5]. As with the use of static line ratings, the use of predetermined, construction model, resistance parameters hinder the effective use of transmission lines. Literature shows that the actual system parameters could be up to 30% off from the values calculated and stored using the construction model [6]. However, with the introduction of PMU devices at the transmission level, it is now theoretically possible to determine real-time dynamic values of resistance. However, several hurdles exist and must be overcome to make this possible.

1.2 Synchrophasor Measurement Units

The switch from traditional SCADA (Supervisory Control And Data Acquisition) based system observations to modern PMU based observations proved to be a significant step towards the modernization of the electric power grid. PMU devices offer substantially superior data acquisition capabilities at much higher sample rates. Furthermore, data from PMU devices are all synchronized such that it is possible to accurately use data from a large network of devices simultaneously without worrying about time lags between the data. PMUs are discussed in more detail in Chapter **Error! Reference source not found.**

Figure 3 draws a comparison between the voltage data obtained using the SCADA system against that obtained from the PMU network of an utility during a disturbance event. As can be seen, the voltage oscillations present during this time period were far less prominently visible with the SCADA data [7].

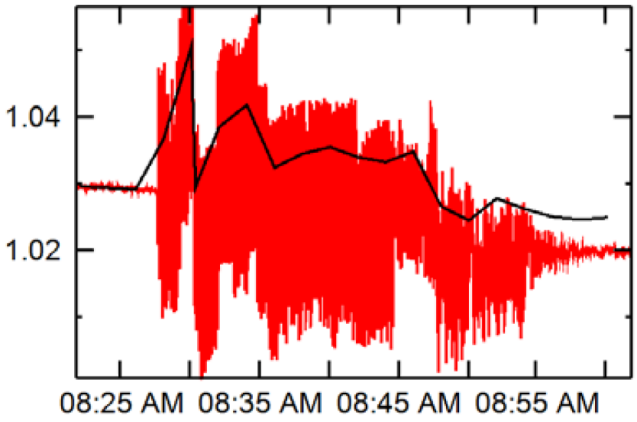

Figure 3. Voltage magnitude (per unit), SCADA and PMU data comparison.

However, this high-resolution data acquisition capability also brings with it several drawbacks, particularly with the permissible ratio of error in the readings. While this error is small enough to not hinder the usefulness of single streams of data, the use of multiple data parameters can compound this error and ultimately make the output unusable. Such is the case when transmission line resistance estimations are obtained using PMU data.

1.3 The Contributions of Proposed Work

Understanding the effect of this inherent error in PMU data, especially when multiple PMU data parameters are used to determine transmission line resistance estimations, and its rectification, such that the said resistance estimations become useful to utilities, forms the motivation for this work. The availability of such, accurate, real-time, line resistance estimations would enable more accurate dynamic line rating estimations as discussed earlier.

A deep dive into the cause of this error is used to formulate a hybrid physics aware learning algorithm that, when applied to PMU data, is able to determine more accurate line resistance estimations. The proposed algorithm consists of an error minimization algorithm based on the physical attributes of the system. The output from this algorithm is then further enhanced through

an Artificial Neural Network (ANN), pretrained to react dynamically to varying system parameters.

The final resistance estimations produced through this process would be usable to a utility due to the significantly lower amplitude for error. A significant factor in this work is the applicability of the proposed algorithm at a sample-by-sample rate without having to use a moving window of samples. This allows the proposed algorithm to be truly real-time or at least match the sampling rate of the data received by the system. An assumption made in this work is that the presence of missing or corrupt data transmitted through the PMU network is not considered. In addition, error due to the intrinsic noise and bias in PMU data as mentioned above is considered and those as a result of uncommon outlier events such as system faults or malicious manipulations.

1.4 Organization of the Dissertation

Chapter 1 provides an introduction to the dissertation and provides a summary of accomplishments. Chapter 2 dives into the development and operation of Synchrophasor Measurement Units and then into the various estimation techniques proposed in literature. Chapter 3 provides the analysis of real PMU data as well as the modeling techniques used. The direct approach to resistance estimation is also discussed and showcased to have issues. Next, Total Vector Error and its effects are discussed in detail and would form the basis for the solution.

Chapter 4 details the proposed correction approach and its sub parts. Chapter 5 includes the numerical analysis of the solution in comparison to the direct method. Chapter 6 provides a conclusion as well as possible future work.

CHAPTER 2

LITERATURE REVIEW

The usefulness of PMU data in the estimation of dynamic line ratings or line resistance estimations is widely recognized in literature. Some notable approaches will be discussed later in this chapter after a discussion regarding the development and operation of PMU devices. The mathematical theory behind phasors is given as Appendix A.

2.1 Adoption of Synchrophasor Measurement Units

The IEEE Standard for Synchrophasor Measurements for Power Systems (IEEE Std. C37.118) [8] governs the fundamental specifications related to synchrophasor measurement units. This section will borrow from this standard as well as some other sources in order to provide the essential basics regarding PMUs.

A. G. Phadke et al. [9] documents the use of microcomputer based Symmetrical Component Distance Relays (SCDR) for the application of real time parameter measurement. The development of the first modern PMU system would later be spearheaded by Phadke and his group of researchers at the Power Systems Research Laboratory at Virginia Tech in the 1980s. The concept was based on years of mathematical methods as well as phase angle measurement techniques proposed in early publications including [10, 11, 12]. The major obstacle at the time was the synchronization of the clocks. [10] and [11] used a radio time signal to synchronize its units while [12] proposed the use of the GOES satellite system that transmits a signal at a fixed rate of 30 pulses per second. None of these systems provided the accuracy required for the technology to be practical. Phadke used the GPS (Global Positioning System) satellites that were coming online at this time for its time synchronization. This proved to have the accuracy as well as the coverage required.

These early prototype PMUs were installed at some substations under the authority of Bonneville Power Administration (BPA), American Electric Power Service Corporation (AEP) and New York Power Authority (NYPA). A collaboration between Macrodyne Inc. and Virginia Tech produced the first commercial PMU in 1991 [13]. With many other manufacturers quickly showing interest in this product, that same year, the IEEE published its first interoperability standard governing the operation of PMUs and the specifications for their data reporting. The standard undergoes revisions in 2005, 2011 and 2014. At the time of this publication, the standard has been incorporated as the IEEE/IEC International Standard - Measuring relays and protection equipment - Part 118-1: Synchrophasor for power systems – Measurements [14]. The IEEE standard defines a PMU as:

"A device that produces Synchronized Phasor, Frequency, and Rate of Change of Frequency estimates from voltage and/or current signals and a time synchronizing signal"

With the United States Department of Energy investing approximately $507 million in the installation of PMU systems nationwide through the Smart Grid Investment Grant Program (SGIG) and other such investments, utilities are increasing their use of these devices on the grid. Over 1350 PMU devices and 226 data concentrators have been installed through this program at its conclusion in 2015. This accounts for approximately 88% of the power load in the country. The program has also been able to achieve its goal of having nearly 100% observability of the high voltage power network in the United States. This includes observability at every interconnection between Independent System Operators (ISOs) [15]. Figure 4 shows the implementation of PMU devices under this program.

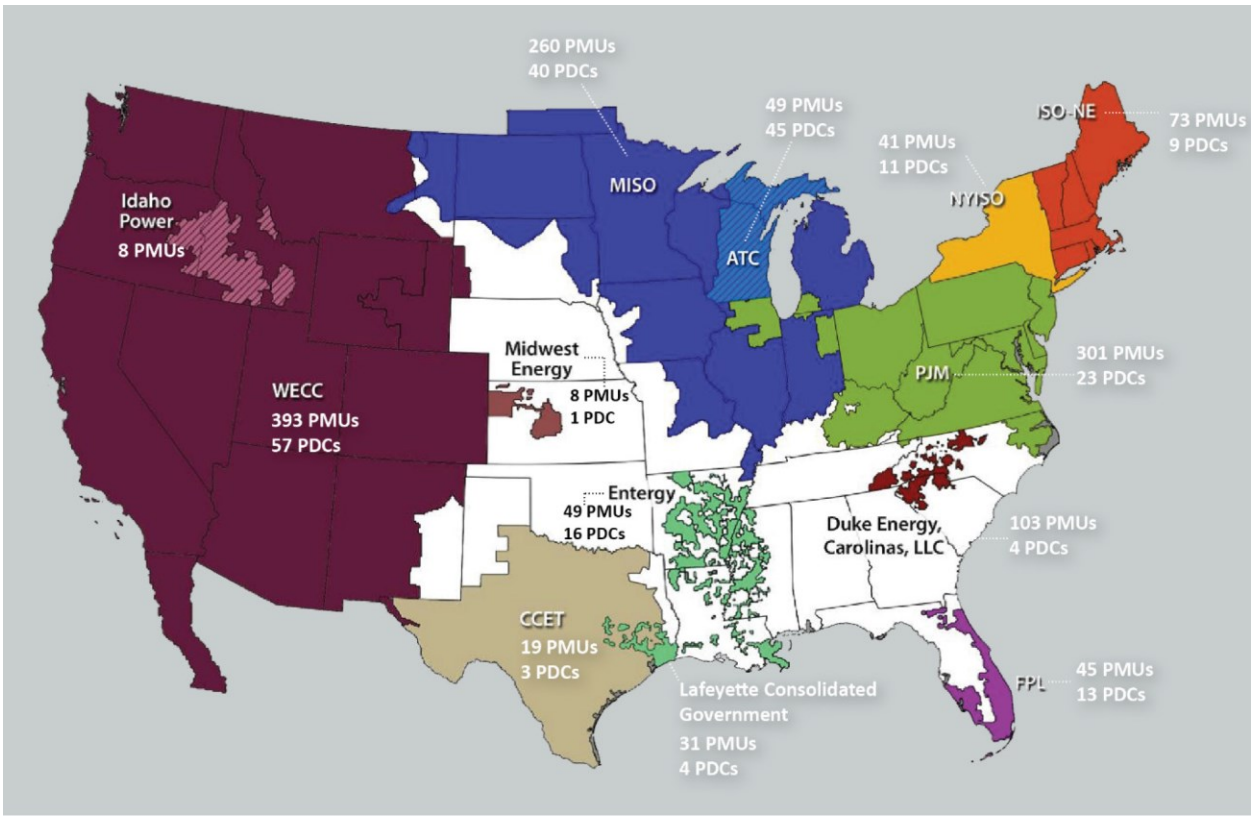

Acronyms: FPL – Florida Power & Light; ISO-NE – Independent System Operator of New England; MISO – Midwest ISO; NYISO – New York ISO; WECC – Western Electricity Coordinating Council

Figure 4. PMU installations through the US Department of Energy, SGIG Project.

Apart from the government grants facilitating the adoption of PMU networks, utilities have also invested heavily in order to gain the benefits of this new technology. However, the costs associated with the implementation of these network have inspired research looking into optimal placement strategies for PMUs to minimize this cost. Studies such as [16, 17] propose methodologies that would minimize the number of PMU installations on the network while ensuring system observability. X. Zhu et al. [18] goes further and also studies the optimal placement of necessary communication infrastructure.

Figure 5, courtesy of the North American SynchroPhasor Initiative (NASPI) and the U.S. Department of Energy, show the adoption of PMUs throughout North America as of March 2015.

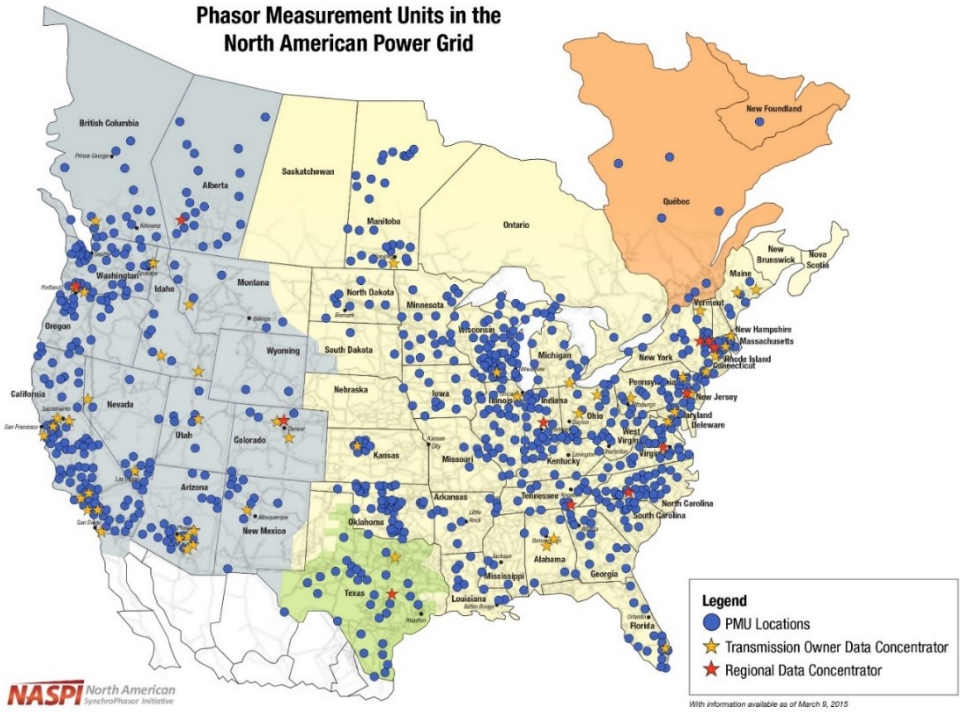

Figure 5. Adoption of PMUs in North America as of March 2015.

PMU systems have proven to be invaluable in providing control centers with good situational awareness and decision support. Also, the fast response rates of PMUs mean that they are also used in protection applications, previously envisioned to be possible, such as in [19] and in recent times to aid in smart fault location operations as in [20]. PMU devices are of 2 basic types that differ in terms of their reporting latency. M-Class devices are intended for accurate system observability whereas P-Class devices are primarily used for protection applications and therefore have a lower latency at the expense of measurement accuracy. For a typical 30 frames per second measurement rate, an M-Class device would have a reporting latency of 166ms while a P-Class would have a reduced latency of 66ms [21].

Due to the dependance of PMU networks on the communication and information infrastructure, concerns regarding cybersecurity and communication reliability have been core avenue of study. The increased complexity and interdependency between the communication and

electrical infrastructure require new models for reliability assessment as discussed in [22]. The effect of cyber threats on PMU networks is also studied in [23, 24]. However, the cybersecurity aspects of PMU networks is beyond the scope of this work and is not incorporated.

2.2 Operation of Synchrophasor Measurement Units

The PMU itself does not measure the transmission line parameters. It is implemented in conjunction with a set of other devices that feed data into it [25]. These include:

- Potential Transformer (PT) or Coupling Capacitor Voltage Transformer (CCVT) for voltage data.
- Current Transformer (CT) for current data.
- GPS receiver for time synchronization.
- Analog to Digital Convertors (ADC). These are often built-it.
- Communications modem.

The setup can be visualized as shown in Figure 6.

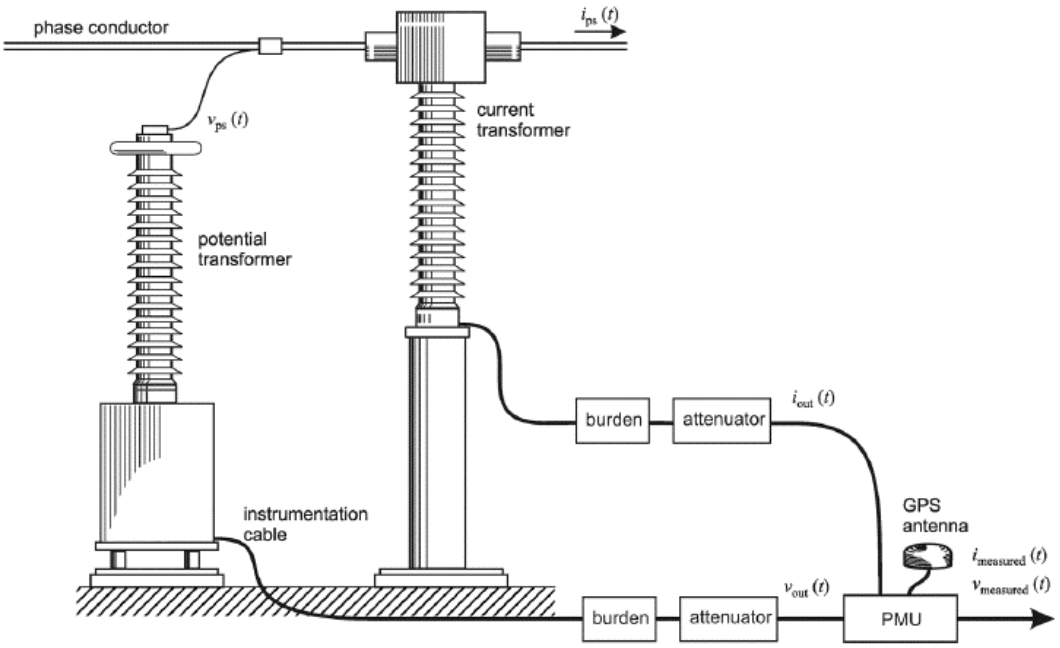

Figure 6. Setup of a PMU system [25].

The time synchronization is achieved with the use of a GPS receiver. This receiver intercepts the Universal Coordinated Time (UTC) broadcasted by the "visible" GPS satellites. The time signal broadcast by GPS is accurate to 2 microseconds and is received every second. A Phase-Locked Oscillator (PLO) then generates the time tags that correspond to the reporting rate of the PMU. However, the time tag reported is not in UTC. Rather, the Second of Century (SOC) format is used. The SOC time is the number of seconds passed since midnight (00:00) of January 1st of 1970. The synchronized time tag consists of 8 bytes during reporting. The first 4 bytes contain the SOC while the next 3 contain a count of the fractions of seconds from the PLO. This frame size can theoretically count with an accuracy of over one 16 millionth of a second. The last byte is a time quality indicator. This total frame size can accommodate SOC values up to the year 2106.

The PMU uses an ADC along with an anti-aliasing filter to generate a digital output. This sampling rate is often higher than the reporting rate of the PMU and this oversampling allows for

better accuracy of the output. The reporting rates that PMU manufacturers must adhere to are laid out in the IEEE standard and are shown in Table 2.

TABLE 2

IEEE STANDARD FOR PMU REPORTING RATES [8]

System Frequency	**50 Hz**		**60 Hz**					
Reporting Rates (frames per second)	10	25	10	12	15	20	30	60

According to the IEEE standard, a PMU must provide data with a Total Vector Error (TVE) of less than 1% under conditions of ±5 Hz off the nominal frequency. The TVE (Ɛ) is defined as "*the square root of the difference squared between the real and imaginary parts of the theoretical actual phasor and the estimated phasor, ratioed to the magnitude of the theoretical phasor*" [26]. This can be given as a percentage as shown in equation (2.1).

$$\varepsilon = \left[\sqrt{\left(\frac{(X_r(n)-X_r)^2+(X_i(n)-X_i)^2}{({X_r}^2+{X_i}^2)}\right)}\right] \times 100 \qquad (2.1)$$

Where X_r and X_i are the theoretical actual synchrophasor values and $X_r(n)$ and $X_i(n)$ are the estimated reported synchrophasor values [13]. r and i standing for real and imaginary respectively.

Minor sources of TVE can result from the burdens within the connection between the measurement transformers and the PMU. However, the most significant source of TVE in the data reported by the PMU is due to the system operating at off-nominal frequencies [13]. For example, if the system frequency is off by 0.2Hz to 59.8Hz, the period of a waveform can increase from 16.666ms to 16.722ms. This will be an increase of over 0.3%. To mitigate these effects, a PMU uses a set of measurement from before and after the reporting time in order to generate an estimated output.

Equations (2.2) and (2.3) show how the estimated one-cycle phasor output $\hat{X}$ is calculated using an N number of cycles [9].

$$\hat{X} = \frac{\sqrt{2}}{N}\sum_{k=-\frac{N}{2}}^{\frac{N}{2}-1} x\left[\Delta t(k+\frac{1}{2})\right] \cdot e^{-j(k+\frac{1}{2})\frac{2\pi}{N}} \tag{2.2}$$

$$\Delta t = \frac{1}{N \times f_{nominal}} \tag{2.3}$$

Where, $x\left[\Delta t(k+\frac{1}{2})\right]$ is the voltage or current measurement at $t = \Delta t(k+\frac{1}{2})$ and $f_{nominal}$ is the system frequency. However, if the frequency at sampling is not equal to the system frequency, equation (2.4) has to be used,

$$x\left[\Delta t(k+\frac{1}{2})\right] = \sqrt{2}Real\left[\bar{X} \cdot e^{-j(k+\frac{1}{2})\frac{2\pi}{N}\cdot\frac{f}{f_{nominal}}}\right] \tag{2.4}$$

where, f is the actual frequency at the time of sampling and $\bar{X}$ is the actual phasor value. By combination and simplification of the above equations, we can obtain an equation for $\hat{X}$ as shown in equation (2.8).

$$\hat{X} = A \cdot \bar{X} + B \cdot \bar{X}^* \tag{2.5}$$

where, $\bar{X}^*$ is the complex conjugate of $\bar{X}$ and,

$$A = \frac{sin\left[\pi\cdot\left(\frac{f}{f_{nominal}}-1\right)\right]}{N \cdot sin\left[\frac{\pi}{N}\cdot\left(\frac{f}{f_{nominal}}-1\right)\right]} \tag{2.6}$$

$$B = \frac{sin\left[\pi\cdot\left(\frac{f}{f_{nominal}}-1\right)\right]}{N \cdot sin\left[\frac{2\pi}{N}+\frac{\pi}{N}\cdot\left(\frac{f}{f_{nominal}}-1\right)\right]} \tag{2.7}$$

Therefore, using equations (2.5), (2.6) and (2.7), we can observe that when $f \rightarrow f_{nominal}$, $A \rightarrow 1$ and $B \rightarrow 0$. Thus, the phasor estimate is very close to the real value as $\hat{X} \rightarrow \bar{X}$. This effect is reversed as the frequency at measurement moves away from the system nominal frequency [13].

According to the standard, a PMU must report phasor estimates for voltage and current as well as local frequency estimates and rate of change of frequency estimates along with a synchronized time tag [27]. Modern PMU devices can report many additional parameters such as circuit breaker and switching statuses. Under standard reporting rates, a single PMU can transmit over 15 GB of data per year.

Apart from the storage bulk, the reporting rate also effects the bandwidth requirements of the communication system. This can be an issue in remote areas without access to a secure high speed communications network. According to a 2010 study by the North American Electric Reliability Corporation (NERC) [28], the bandwidth requirements can increase rapidly with an increase in the number of PMUs in the system as well as based on their reporting rate. Some approximate bandwidth requirements are as shown in Table 3.

TABLE 3

APPROXIMATE BANDWIDTH (KBPS) REQUIREMENT FOR A PMU NETWORK

Reporting Rates (frames per second)	**Number of PMUs**			
	2	**10**	**40**	**100**
10	14	55	209	521
15	29	110	418	1043
30	57	220	836	2085

2.3 Phasor Data Estimation Techniques

As detailed earlier, data from a PMU needs to be processed for errors and outliers. This is achieved by some form of estimation technique as has been thoroughly studied in the literature. The basic idea can be derived from earlier publications such as [29] where the concept of state estimation is well defined. However, this was during a time before PMUs were widely available.

More recent publications such as [30, 31] explore how the accuracy of these new technologies can be supplemented by the use of state estimation on the outputs. [32, 33] propose novel methods of using a hybrid estimation system that makes use of a limited number of PMUs available to supplement the data from widely available SCADA systems to improve accuracy. However, the goal of this and other recent literature is to not rely on additional data sources apart from the PMU network.

[34], [35] and other similar studies use these ideas to implement a state estimation algorithm, for line impedance calculation, making use of the PMU network on the Croatian transmission power system. The findings of these papers show that while state estimation can produce accurate outputs by eliminating random noise and outliers, their effectiveness only increase with an increase in the number of successive samples processed. This increases the processing time and introduces delay.

2.4 Dynamic Line Rating and Resistance Estimation based on PMU Data

D. L. Alvarez et al. [36] reviews the application of Dynamic Line Rating using PMU data as well as the benefits and challenges faced. Figure 7 showcases applications where DLR information would be useful to a utility. These varies from time sensitive operations, such as during contingencies, to daily safe operations to long term expansion gird plans. The inefficiencies due to static line ratings is also stressed. The authors also note that the availability of accurate dynamic resistance estimations by way of PMU data would enable addiotnal applications such as the estimation of conductor temperature and line sag and would improve overall system reliability.

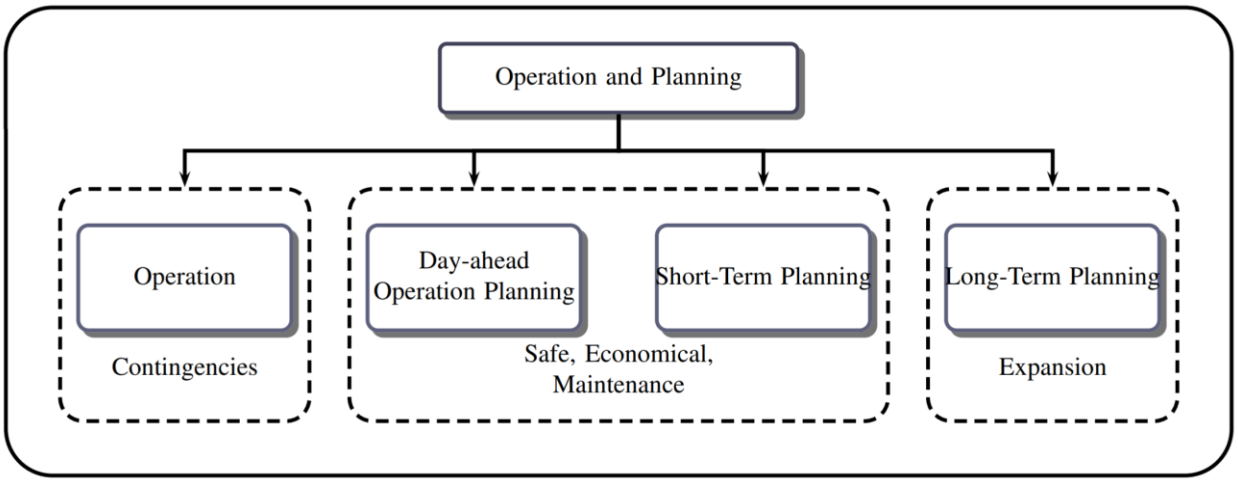

Figure 7. Applications of DLR [36].

However, for the estimation dynamic line ratings, the error issues mentioned previously regarding the estimation of primary PMU data are further compounded by the adverse effects of TVE that must also be accounted for. A viable solution to this has been a goal of utilities and researchers alike. A study conducted by Idaho Power in 2015 concludes that when, non-simulated, real data is used, resistance estimations from both the PMU and SCADA based systems studied "*exhibit significant variability and sometimes deliver unreasonable results"*. This included negative results for line resistance [37].

D. Shi et al. [38] propose the use of calibration factors obtained with knowledge of actual impedance values of the line using measurement sensors. These calibrations must be repeated often and, based on the analysis on real data, the bias error would be far too dynamic for repeated calibrations to be a viable solution. In addition, this solution requires additional physical equipment to be attached to lines periodically. C. Pisani et al. [39] propose a modification to [38] with the use of an addiotnal constrained nonlinear programming approach to support with the PMU bias. The authors stress the need for better DLR observability with the increase in renewable sources and the resulting underutilization of lines. Authors also observe that when the line current falls below

a certain threshold value, the effect of the calibration process in compensating the highlighted PMU issues is weakened. Hence, in low line loading conditions, the behavior of the transmission line model is unpredictable and tends to deviate massively from the expected values. Similar behavior is also observed in this work when analyzing the available PMU data.

Prostejovsky et al. [40] take an alternate approach to the problem of measurement tolerances and noise by considering micro-PMU devices found at the distribution level. Instead of typical PMU based estimation approaches that require precise phasor data, the proposed approach would only consider the magnitudes of voltage and power as well as the quadrant in which the phasor exists. A compensation model is then used to account for measurement errors. The applicability of the proposed least squares (LSQ) minimization approach is demonstrated on simulated data. However, regardless of the implementation at the distribution or transmission level, the use of PMU data while only considering measurement errors due to noise with an assumed gaussian distribution is not realistic in the known presence of non-Gaussian bias error. Biasness and non-Gaussian nature of the measurement data has been investigated and proven in literature such as [41], and the need for a methodology that effectively deals with it is emphasized.

D. Ritzmann et al. [42] propose that accurate estimated parameter values would be essential in improving the performance and reliability of a range of power system applications including monitoring, protection [43, 44], stability [45, 46], control [47, 48], fault detection and location [49, 50] and dynamic thermal line rating. Authors also claim that PMUs often exceed the requirements of 1% total vector error (TVE) limitations set by the governing standard. The proposed least squares based estimation technique utilizes constant systematic errors and tests are only conducted over short periods of time on simulated data and would struggle with real PMU data consisting of more dynamic errors and biases.

R. S. Singh et al. [51] demonstrate the need for accurate estimates of real-time resistance of transmission lines as these estimations would be valuable in dynamically determining the temperature of the line conductors. A primary constraint in routing extra power through a line is its thermal rating. Particularly, in the case of underground cables where the insulation is very sensitive to excessive temperatures. Authors also propose that transmission lines connecting large wind or solar farms to the main grid might act as a bottleneck in the system during periods of peak output and thus, in order to simplify the calculation of dynamic line resistances, the effect of random Gaussian measurement and estimation errors in PMUs may be mitigated using a longer data window. However, this approach does not deal with the inherent bias error present in PMU data.

D. Alvarez et al. [52] and L. Dawson et al. [53] propose a dynamic conductor temperature estimation methodologies that take into account a range of factors including real time current flow, line sag, as well as the input from ambient temperature sensors. The methodology is proposed as a solution for the inefficiencies of using preset, conservative, values for line limits. However, for line resistance, construction values are used. The temperature estimation would benefit further if dynamic resistance values were also incorporated. M. K. Hasan et al. [54] propose such an improvement with the use of PMU data for the calculation of dynamic line resistances. The authors assert that large current flows through a transmission line may cause it to reach up to its maximum flow limits and thus, lead to an increase in the conductor temperature. This thermal effect would degrade the performance of the transmission line and, as a result, would decrease its power efficiency. However, in their proposed DLR algorithm, the authors do not take into account the biasness of the error found in PMU data.

D. Gurusinghe et al. [55] make the claim that a large portion of PMU data based estimation approaches and calculation techniques proposed in literature use offline or synthetic data that do not react appropriately to the realities of the environmental factors and loading conditions seen when real PMU data is used. The authors also state that utilities currently use constant, theoretical values for line parameters based off of construction data that consist of numerous approximations leading to inefficient use of transmission line capacities. D. Gurusinghe et al. also state that while the Gaussian noise existing in PMU data could be accounted for using a number of techniques, the bias error in PMU measurement is difficult to eliminate using these techniques.

A. Riepnieks et al. [56] brings forth the idea of comparing signals received from the PMU against their counterpart calculated using other signals also obtained from the PMU and fed though a physics-based model. This concept is further developed in this work to compare, not the received signals but, the estimated system parameters against a physics-based model.

CHAPTER 3

ANALYSIS OF PHASOR DATA AND TOTAL VECTOR ERROR

An imperative aspect of this research is that all techniques and models proposed have been developed and tested with the use of a real synchrophasor measurement data from a large Mid-Western utility that operates over 200 PMUs across their transmission area.

3.1 Availability of Data

Synchrophasor data was available from 230 PMU devices that geographically spanned an entire state in the United States. The data was available in single phase for 13 months and in 3 phase for 10 months. The reporting rate of the PMUs was 30 times per second.

The single-phase PMU data consists of a record of 10 parameters from each PMU while the three-phase PMU data consists of a record of 23 parameters from each PMU. A list of the parameters contained in each record is shown, for the case of single-phase and three-phase, in Appendix A and Appendix B, respectively.

3.2 Transmission Line Modeling

Multiple lines of varying lengths were used in this work. This allowed all proposed algorithms to be checked against variations in line length, conductor types and line parameters. The typical data for a particular line is detailed below. For this 345kV, 70-mile line, the PMU setup at each end of the transmission line consisted of a CCVT for voltage measurements and a CT for current measurements. Additional information according to the CAPE (Computer-Aided Protection Engineering) model is as given in Table 4. The line impedance and admittance values are given according to the CAPE Model physical calculations. These are the construction values detailed earlier.

TABLE 4

CAPE MODEL PARAMETERS FOR TRANSMISSION LINE

Parameter	**Value**
Phase	3 Phase
Nominal Voltage	345 kV
Length	72.01 miles
Line Resistance in positive sequence	3.970072 Ω
Line Reactance in positive sequence	53.70414 Ω
Line susceptance in positive sequence	420.4561 μʊ

3.3 Line Resistance Modeling

For modeling of the transmission line, a nominal pi model was used. Typically, such a model for transmission line is used when the length of the line ranges from 50 to 150 miles. A majority of the lines in the network studied falls well within this range and the use of this model for even shorter lines only adds to the accuracy. The use of this model is also necessary as the shunt admittance of the line is not ignored but rather lumped together along with the line impedance. For lines of this length, effect of shunt admittance must be accounted for in the estimation of accurate impedance parameters. A diagram of the proposed model is as shown in Figure 8 [57]. The sending end voltage and current, V_S and I_s respectively, and receiving end voltage and current, V_r and I_r respectively, will be used for the calculation of the impedance, Z. The Kirchhoff's law-based equations given in equation (3.1) will be used for this calculation [42]. Since this work is primarily interested in the resistance estimation, R^e, of the line, the real part of Z is used as shown in equation (3.2). The reactance, X, for the line can be obtained by taking the imaginary part of Z [57].

$$Z(n) = \frac{V_s^2 - V_r^2}{V_s I_r + V_r I_s} \tag{3.1}$$

$$R^e(n) = real(Z(n)) \tag{3.2}$$

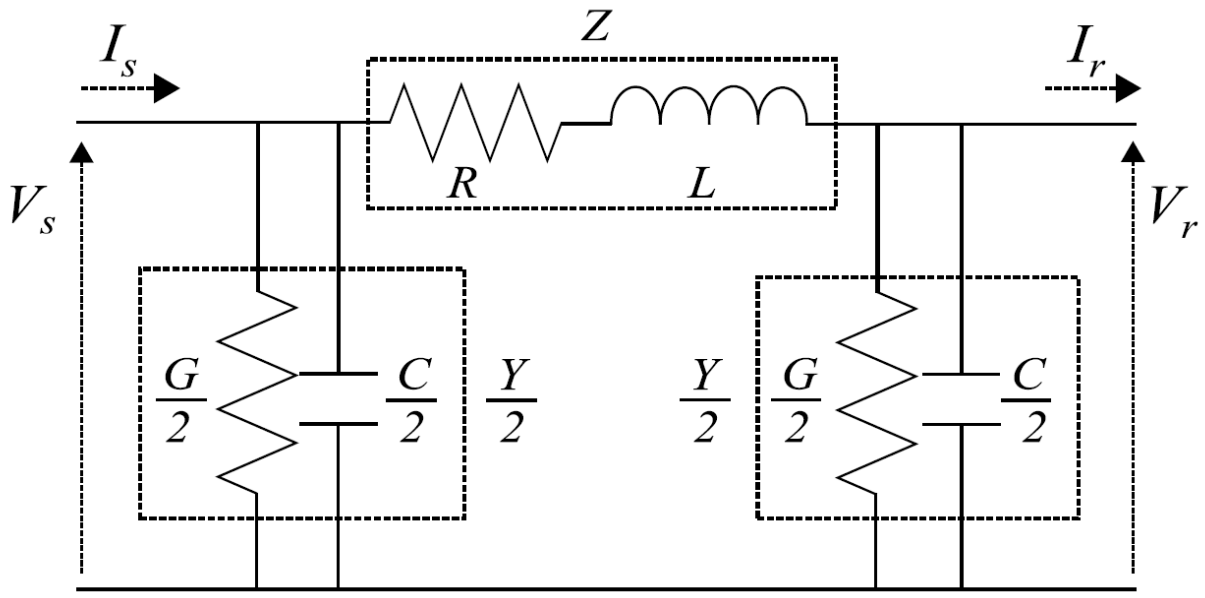

Figure 8. Pi model of medium line transmission lines [42].

3.4 Data Obtained from Synchrophasor Measurement Units

The data supplied by the utility consist of an individual file for each minute of data. The data is contained in a *.phasor* compressed file format and needs to be decompressed using proprietary software. Decompressed, the data is contained in a *.csv* format with columns as given in section 4.1. Bespoke Matlab algorithms were written to streamline the data extraction process and to allow any amount of data to be extracted and decompressed as needed. This is necessary as, due to the immense size, it is only possible to have a small amount of data in uncompressed form at any time.

3.4.1 Basic Phasor Data

Figure 9 and Figure 10 show a 1-minute section of voltage magnitude values and 1-minute section of current magnitude values, respectively, obtained from the PMU data. The sampling rate is 30 times a second and therefore this section contained 1800 samples.

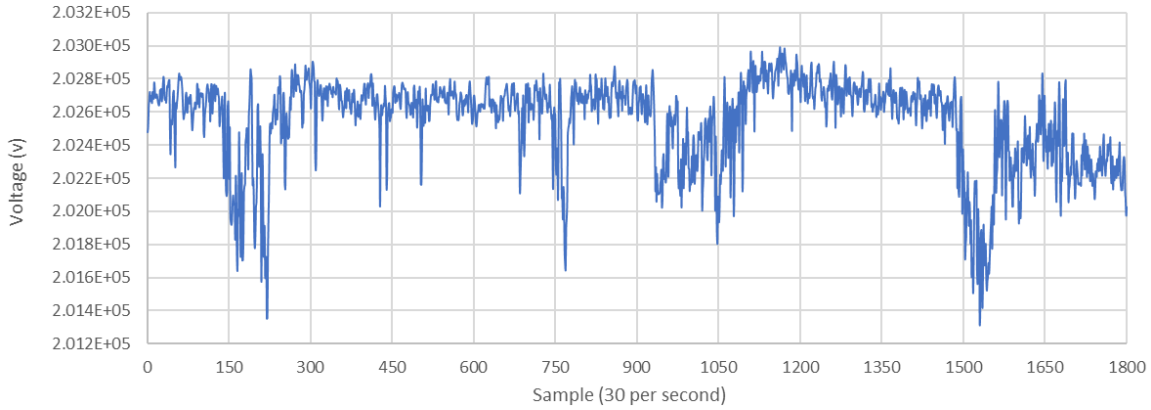

Figure 9. Voltage magnitude over a minute.

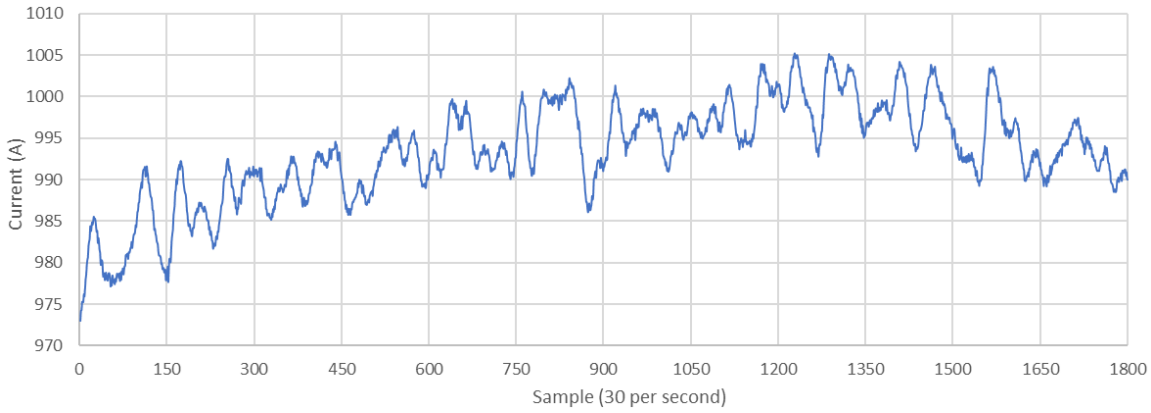

Figure 10. Current magnitude over a minute.

Since the voltage and current data obtained from the PMU is given as magnitude, V_{mag} and I_{mag}, and phasor angle, V_{ang} and I_{ang}, the equation (3.3) is used to convert this data into complex form. x is either sending end, s, or receiving end, r.

$$V_x = \left(V_{x_{mag}} \times cos\, V_{x_{ang}}\right) + j\left(V_{x_{mag}} \times sin\, V_{x_{ang}}\right) \tag{3.3}$$

3.4.2 Analysis of Line Reactance and Resistance

Using the equations presented earlier, the reactance and resistance is calculated. Note that this is done with the use of data from 2 PMUs on either end of a transmission line. Figure 11 shows the reactance information obtained and Figure 12 shows the resistance information obtained. In both graphs, it is evident the mean values lie close to what is expected according to the construction values given in Table 4. This section of data can be considered a very good section where the output values are close to what is expected. However, at other times this is not the case. While the reactance values can be seen to always hover close to the expected values, the resistance can be observed to vary greatly. This forms the motivation for this work.

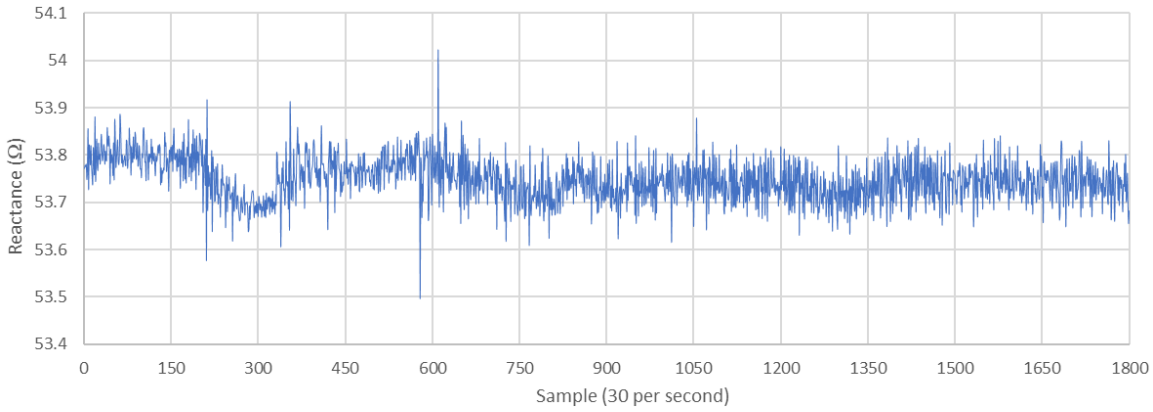

Figure 11. Reactance over a minute.

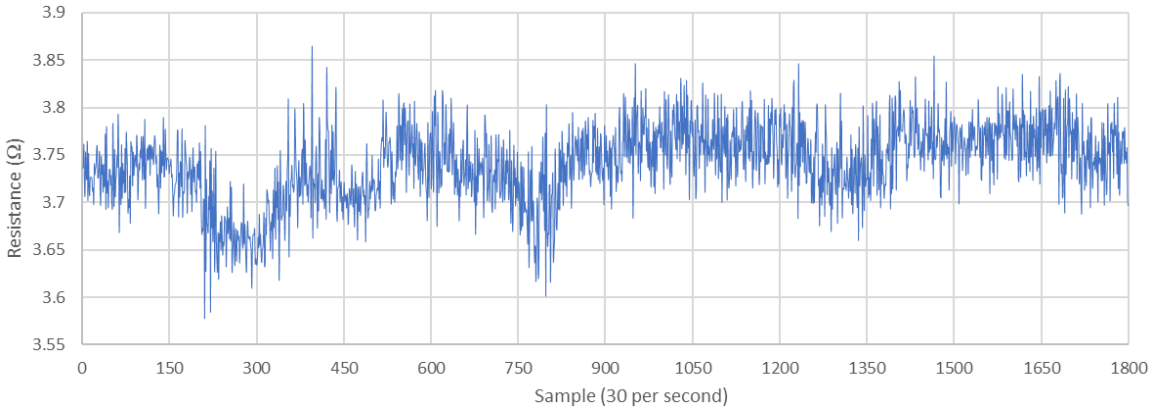

Figure 12. Resistance over a minute.

3.4.3 Analysis of Line Resistance with Varying Conditions.

As stated in the previous section, the resistance calculated from PMU data can be seen to vary greatly from what is expected. To try and find some kind of correlation to any other physical factor, an expansive study was conducted. The avenues that initially showed promise were the correlation of resistance deviation with the current magnitude in the line as well as with the length of the line. Figure 13 shows a sample of some of the tests conducted. From observation of many such plot, it is possible to come to some conclusion.

- In medium lines carrying a high current, the calculated resistance come, in most cases, close to what is expected according to the construction model. This can be seen in row 1 of Figure 13.
- In medium lines carrying a low current, the calculated resistance can vary. It can sometimes reach values far higher than possible. The resistance was also observed to go slightly into the negative regions. This can be seen in row 2 of Figure 13.
- In short lines carrying a high current, the calculated resistance can vary greatly. Again, reaching values far higher than possible as well as deeper into the negative regions. This can be seen in row 3 of Figure 13.
- In short lines carrying a low current, the calculated resistance is shown to be highly erratic and completely unusable. This can be seen in row 4 of Figure 13.

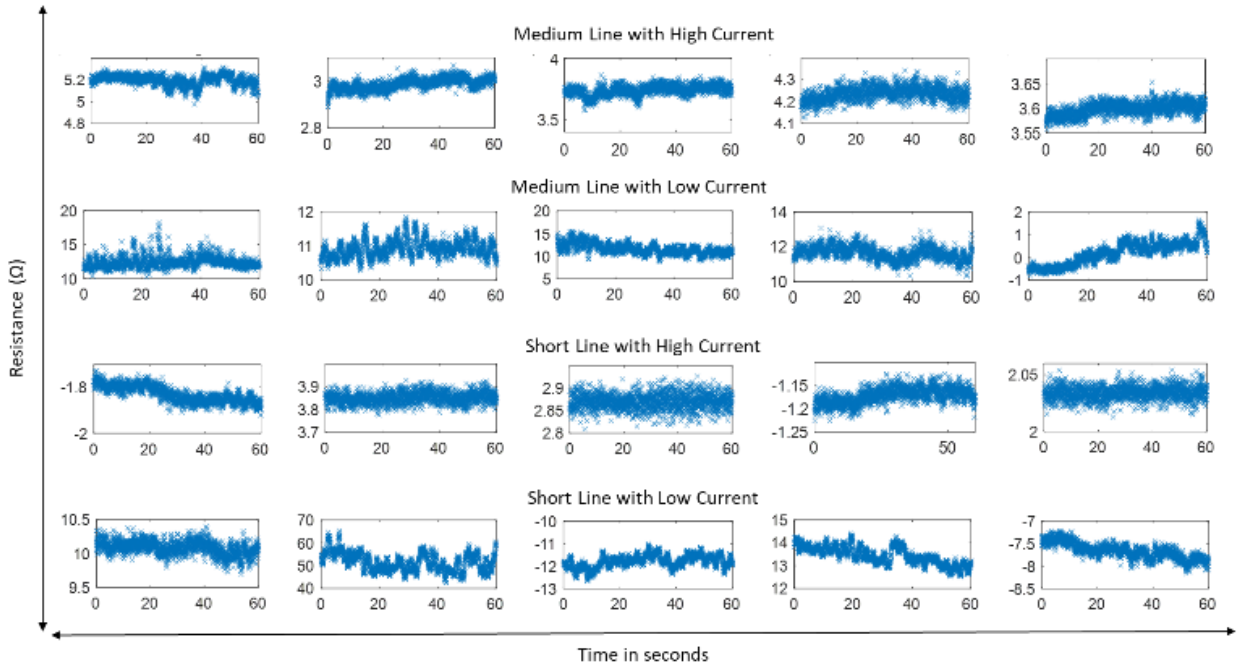

Figure 13. Variation of resistance due to line length and line current.

3.5 Error Correlation to Line Current

To further investigate the phenomenon observed in section 4.3.3, a larger study was done to observe the variation of calculated resistance against the line current flow. Approximately 10,000 random, discontinuous, points of time were selected. This includes all seasons, times of day as well as environmental conditions. For each point, the estimated resistance as well as the percentage error between this estimated resistance and the construction model resistance was obtained. These points were then plotted against the current flow, as a percentage of its current capacity, in the line at the time.

Several tests, utilizing multiple lines of varying lengths, were conducted. All tests showed a consistent result similar to what is shown in Figure 14. As can be seen, when the line current is high, the calculated resistance output is very similar to what is expected according to the construction model. However, as the line current is decreased, the region of error for the calculated

resistance grows significantly. Essentially, as the line current reaches closer to the current capacity of the line, the observed deviation is reduced.

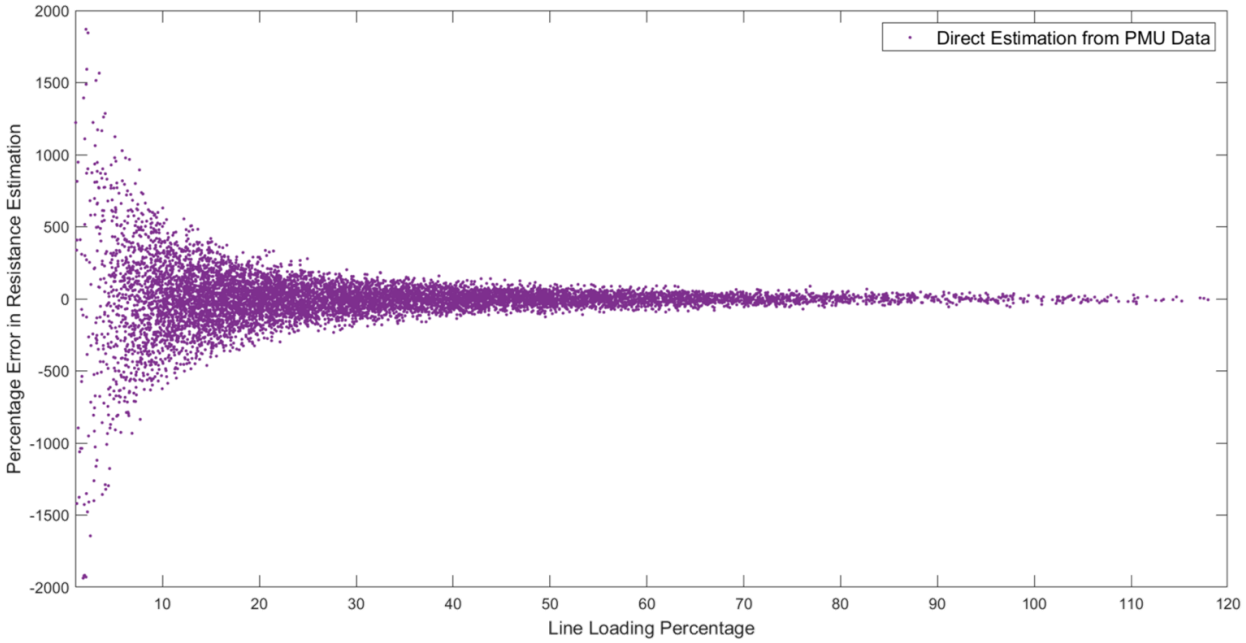

Figure 14. Percentage resistance error against percentage line loading.

3.6 Investigation of the Effect of Total Vector Error

Figure 14 showcases the effect line current has on the viability of resistance calculations done using PMU data. The first objective of this work is to understand the fundamental reasoning behind this large variation.

After some initial discussion with our utility partners, Current Transformer (CT) saturations was put forward as a possible reason for this effect. To investigate this, CT correction information was obtained from the utility and the appropriate correction factors were included in the resistance calculation. However, it was evident that within the region of our current data, CT based error was negligible.

The next avenue of investigation was with the Total Vector Error (TVE) in the obtained PMU data. A fundamental understanding of TVE is necessary for this. The IEEE Standard C37.118

states that a PMU device must provide vector data with a TVE of less than 1% under normal system frequency conditions. Normal conditions being the system operating within ±5% of the normal frequency. The standard defines TVE as "the square root of the difference squared between the real and imaginary parts of the theoretical actual phasor and the estimated phasor, ratioed to the magnitude of the theoretical phasor". Equation (3.4) represents this relationship [8].

$$TVE(n) = \sqrt{\frac{\left(X_r^e(n) - X_r^a(n)\right)^2 + \left(X_i^e(n) + X_i^a(n)\right)^2}{\left(X_r^a(n)\right)^2 + \left(X_i^a(n)\right)^2}} \tag{3.4}$$

where n is the sample number, X^e and X^a are the estimated and actual vectors, respectively, and r and i denote the real and imaginary components, respectively, when a vector is represented in complex form.

The TVE can also be broken down into its magnitude and phasor angle components. The relationship of these components to the TVE is shown in equation (3.5) [58].

$$TVE(n) = \sqrt{2(1 \pm \lambda)(1 - cos\,\gamma) + \lambda^2} \tag{3.5}$$

where, λ is the magnitude error and γ is the phasor angle error. Independent analysis of each of these errors provides the maximum tolerable values for them. Thus, to maintain an overall TVE of 1%, the maximum allowable value for phasor angle error, $\gamma = \pm 0.573°$. The maximum allowable value for magnitude error, $\lambda = 1\ pu$. TVE is a function of both magnitude error and phase angle error and therefore the maximum corresponding errors of each can be visualized for each TVE percentage as shown in Figure 15 [59].

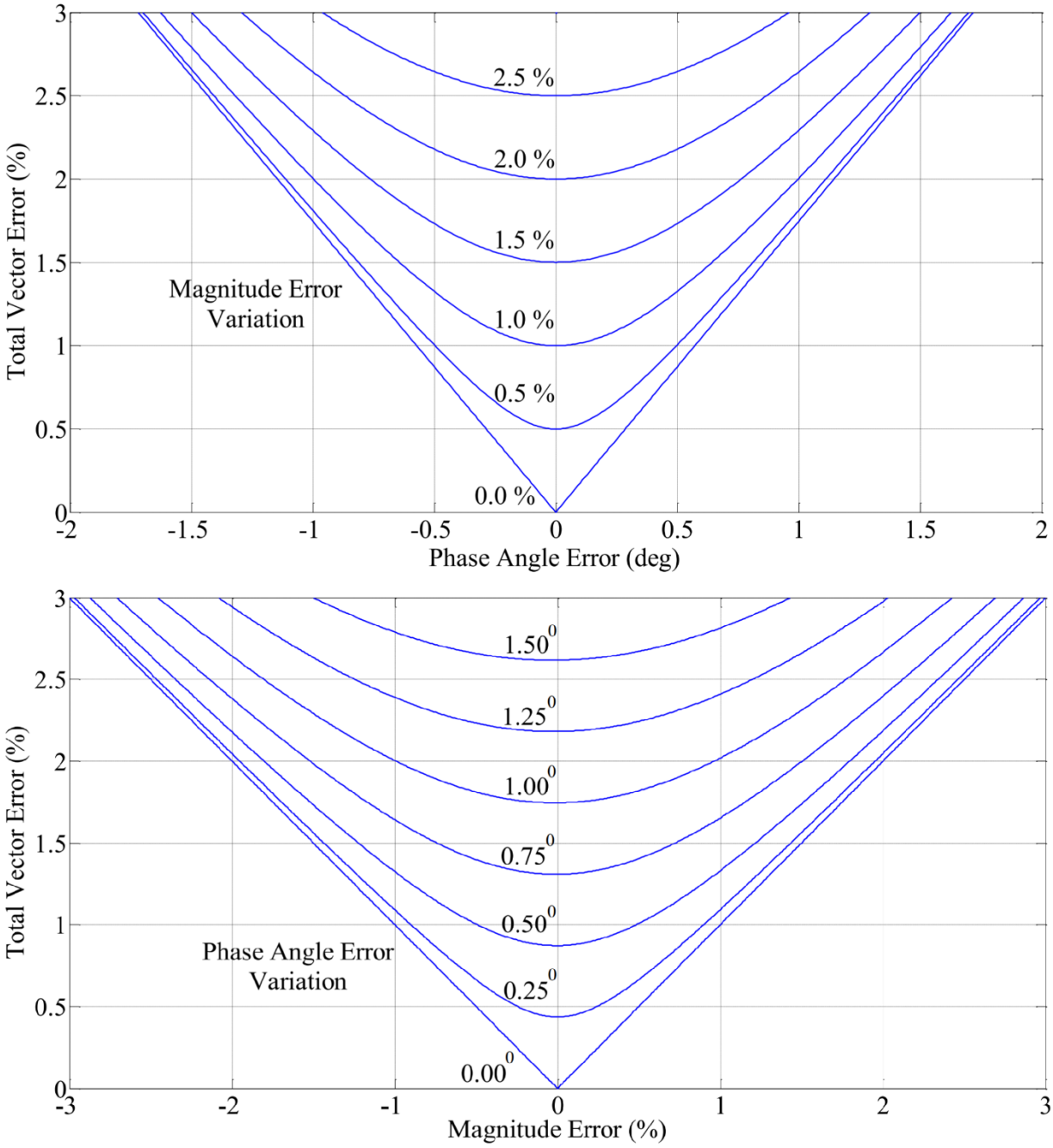

Figure 15. Visualizing TVE as a function of magnitude error and phase angle error [59].

3.6.1 Visualization of Total Vector Error

Based on the findings regarding TVE, it is possible to visualize TVE in vector space as shown in Figure 16. In the figure, r_a represents the actual phasor magnitude for a particular line parameter and θ_a represents its phasor angle. Dashed circle would represent a limit of 1% of TVE. Note that the size of the circle has been exaggerated for clarity. Therefore, if the PMU device outputs its estimate for this particular parameter as the phasor r_e with a phasor angle of θ_e, it would fall within the TVE error range and would be perfectly acceptable as an estimate. Conversely, if r_e fell anywhere outside the dashed circle, the estimate would not be valid.

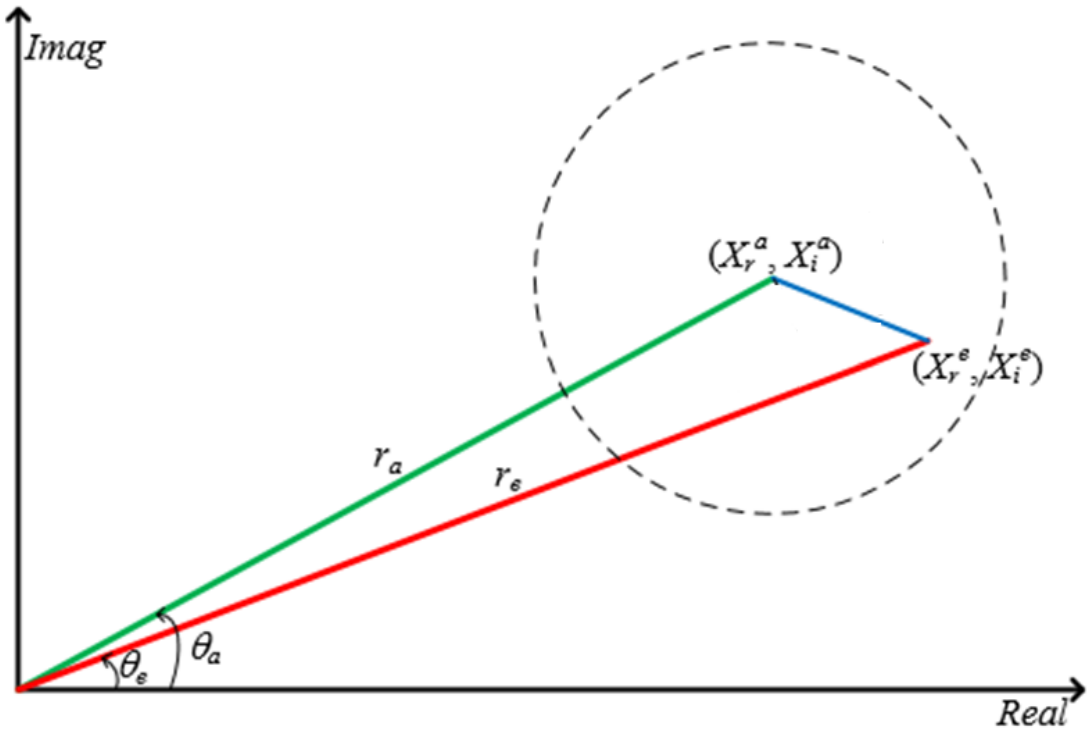

Figure 16. Visual Representation of TVE.

Analysis of real PMU data obtained from a utility shows that, as expected, these errors are barely detectable when observing a single data stream. However, all data that is obtained can be

represented in the forms in equations (3.6) and (3.7) where r and θ are the line parameter's magnitude and phasor angle and e and a denote estimated and actual values respectively.

$$r_e(n) = r_a(n) + \lambda(n) \tag{3.6}$$

$$\theta_e(n) = \theta_a(n) + \gamma(n) \tag{3.7}$$

TVE present in PMU data rarely causes a problem when observing a single data stream. The number of line parameter data obtained from a single PMU is limited to some basic properties such as the voltage phasor, current phasor and frequency. It is possible, however, to make use of these simple properties from 2 or more PMU devices to extrapolate additional system parameters such as transmission line resistance. However, this is where the presence of TVE plays a major role in providing incorrect estimates. The cause of these large errors in calculated system parameters data is studied next.

Figure 17 shows the interaction between 2 phasors at a particular sample time. The 2 phasors could represent data from 2 PMU devices such as the voltage readings from PMUs on either end of a transmission line. (r_{a1}/θ_{a1}) represent the actual phasor 1 and (r_{a2}/θ_{a2}) represent actual phasor 2. The 2 dashed lines show the permissible TVE for either phasor. Therefore, the PMU estimates for either phasor, (r_{e1}/θ_{e1}) or (r_{e2}/θ_{e2}) can be seen to fall within the acceptable TVE regions of its respective phasor. However, it is evident here that a problem has unearthed. The difference vector between the actual phasor and the one between the estimated vectors can be seen to be vastly different from one another. Therefore, any calculations that would rely in this difference vector would see large errors in its estimations. The possible percentage of magnitude error and the possible angle error due to this phenomenon can be calculated as shown in Table 5 and would be different for vector addition and subtraction.

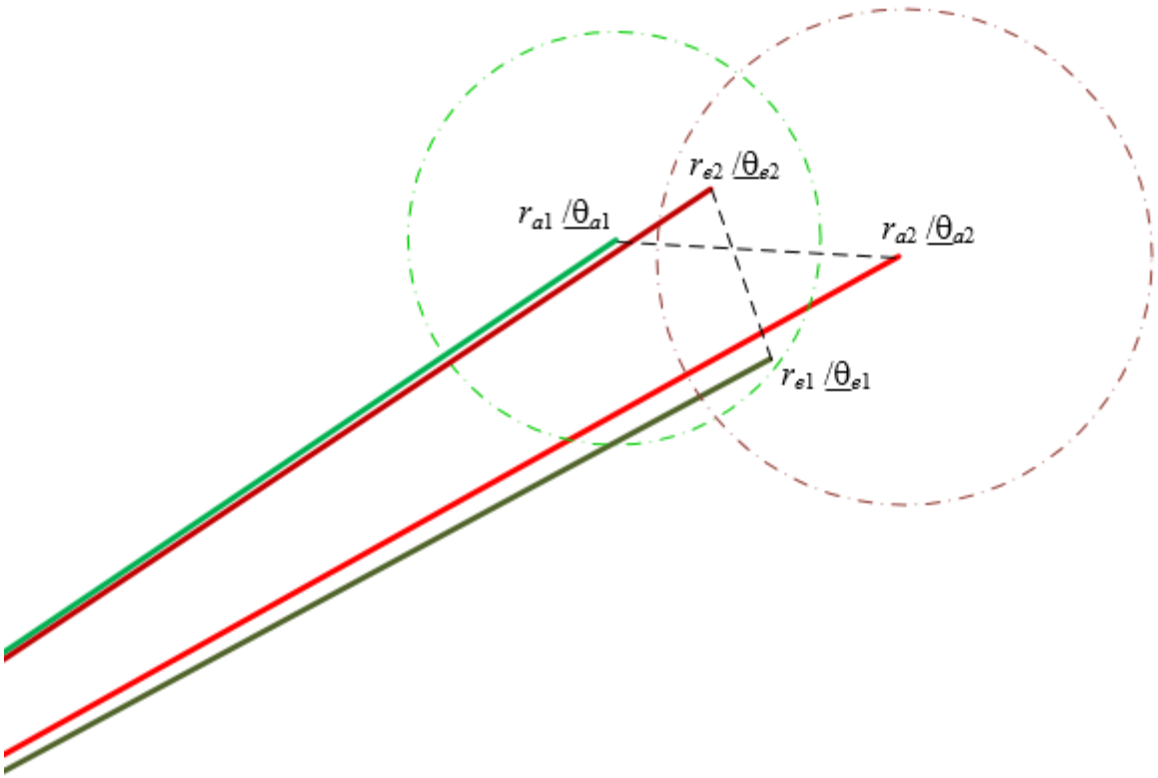

Figure 17. 2 Phasors with intersecting TVE.

TABLE 5

POSSIBLE PERCENTAGE OF MAGNITUDE AND ANGLE ERROR ON VECTORS

Operation	**% Magnitude Error**	**Angle Error**
Addition	$\frac{0.01(\lvert r_{a1}\rvert + \lvert r_{a2}\rvert)}{\lvert r_{a1} + r_{a2}\rvert}100\%$	$\pm\cos^{-1}\left(\frac{(r_{a12})^2 + (r_{e12})^2 - (r_{ae12})^2}{2r_{a12}r_{e12}}\right)$
Subtraction when $\lvert r_{a1} - r_{a2}\rvert \geq 0.01(\lvert r_{a1}\rvert + \lvert r_{a2}\rvert)$	$\frac{0.01(\lvert r_{a1}\rvert + \lvert r_{a2}\rvert)}{\lvert r_{a1} - r_{a2}\rvert}100\%$	$\pm\sin^{-1}\left(\frac{(\lvert r_{a1}\rvert + \lvert r_{a2}\rvert)}{\sqrt{((r_{a1})^2 + (r_{a2})^2 - 2r_{a1}r_{a2}\cos(\theta_{a1} - \theta_{a2}))}}\right)$
Subtraction when $\lvert r_{a1} - r_{a2}\rvert < 0.01(\lvert r_{a1}\rvert + \lvert r_{a2}\rvert)$	$\frac{0.01(\lvert r_{a1}\rvert + \lvert r_{a2}\rvert)}{\lvert r_{a1} - r_{a2}\rvert}100\%$	$\pm 180°$

Table 5 provides an interesting conclusion. It can be seen that calculations involving the addition of vectors would result in only minor errors. However, calculations that rely on the subtraction of vectors would result in much larger and significant errors in estimations. It can also be deduced that the distance between the 2 actual vectors has an influence on the amount of error possible in the estimates. If the TVE boundaries of the vectors do overlap, the possible angle error is ±180°. These are the instances where a majority of large errors would be observed. This can be seen by observing Figure 17 and Figure 18.

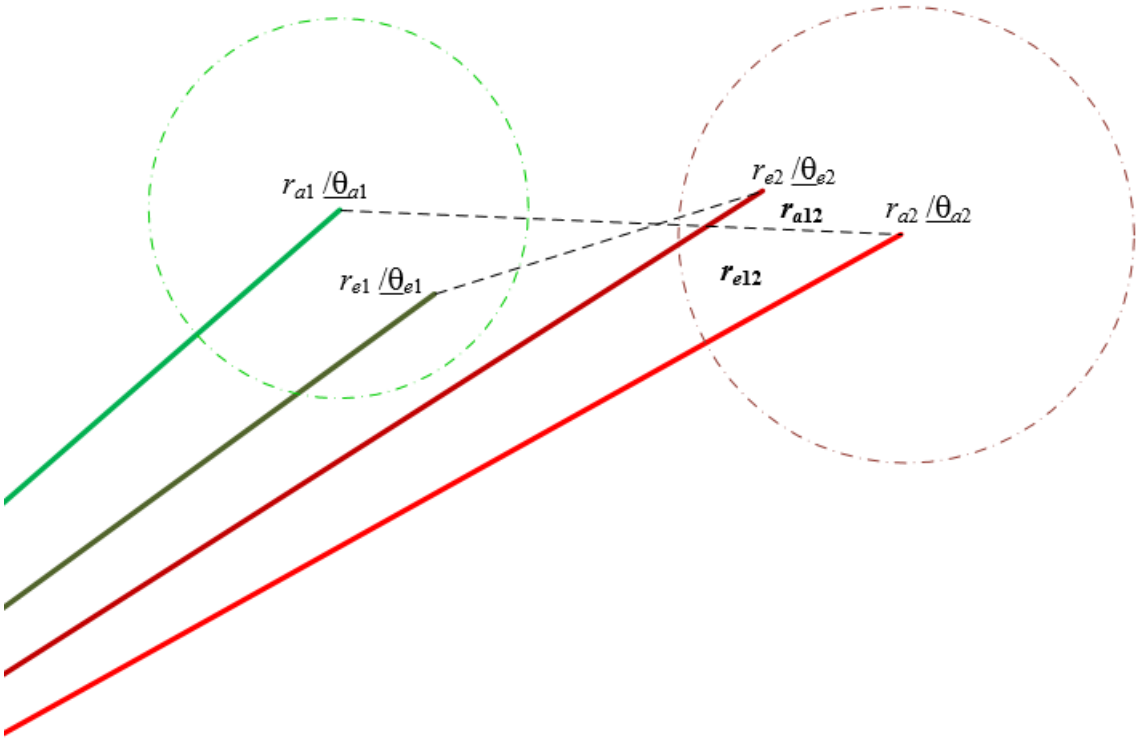

Figure 18. Interaction of 2 far-away vectors.

In Figure 17, the presence of the 2 vectors in close proximity to each other provides a larger area in which the TVE regions of the 2 actual vectors intersect. This also means that the possibility of the difference vector between the 2 estimated vectors being highly different from the difference vector between the 2 actual vectors is much higher. As seen in the scenario in Figure 17 the

estimated difference vector is completely reversed and, in some cases, can be up to a 180° off. Figure 18 on the other hand shows 2 vectors further away from each other in the vector space. Here, the TVE regions do not intersect and therefore the disparity between the 2 difference vectors is fairly limited. In these cases, it can be expected that the resulting estimates would contain a lesser error.

Furthermore, it can therefore be deduced that, since the possibility of error relates to the possibility of the vector TVE regions overlapping, in the application of resistance estimations, the possibility of error would relate to the distance between the sending and receiving voltage vectors in the vector space. Also, the error would be further amplified due to the squaring done in the calculation as seen in equation (3.1). This phenomenon therefore justifies the variation of calculated resistance seen in Figure 14. As the line loading reduces, the distance between the voltage vectors would also reduce and therefore the overlapping possibility increases. In addition, it is also reasonable to assume that the length of the transmission line would also have an effect as shorter lines would have a smaller difference in voltage across them. The observation that error is more prevalent in shorter transmission lines has in-fact already been made in literature [60].

3.6.2 Mathematical Recreation of Total Vector Error

A mathematical approach is taken to observe the interaction between 2 vectors in the presence of TVE. The first step of this approach was to recreate TVE based intrinsic error mathematically. For this, a large number of normalized vector pairs are created based on statistical data from the real-world system. For each of these vectors, their 1% TVE boundary is also created. A sampling of a few of these is shown in Figure 19. As can be seen, the deviation between the pairs would differ as shown in Figure 19 with a number of these pairs consisting of overlapping TVE boundaries. Next, a large number of estimates with TVE are obtained for each vector pair.

These estimates would be random points within the TVE boundaries of each vector. A small sampling of these estimated for just a single vector pair is shown in Figure 20.

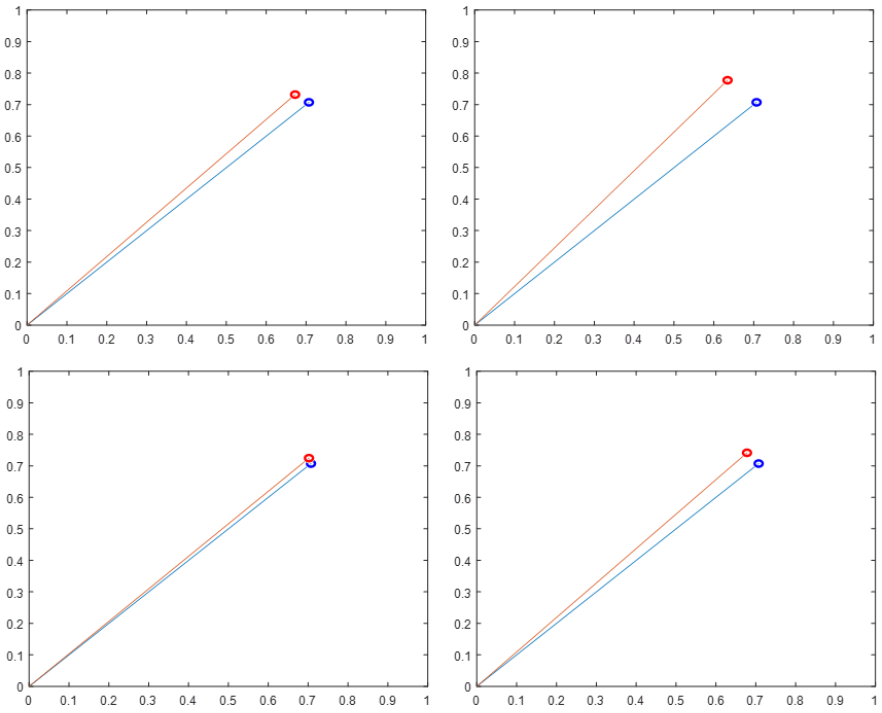

Figure 19. Sample vector pairs.

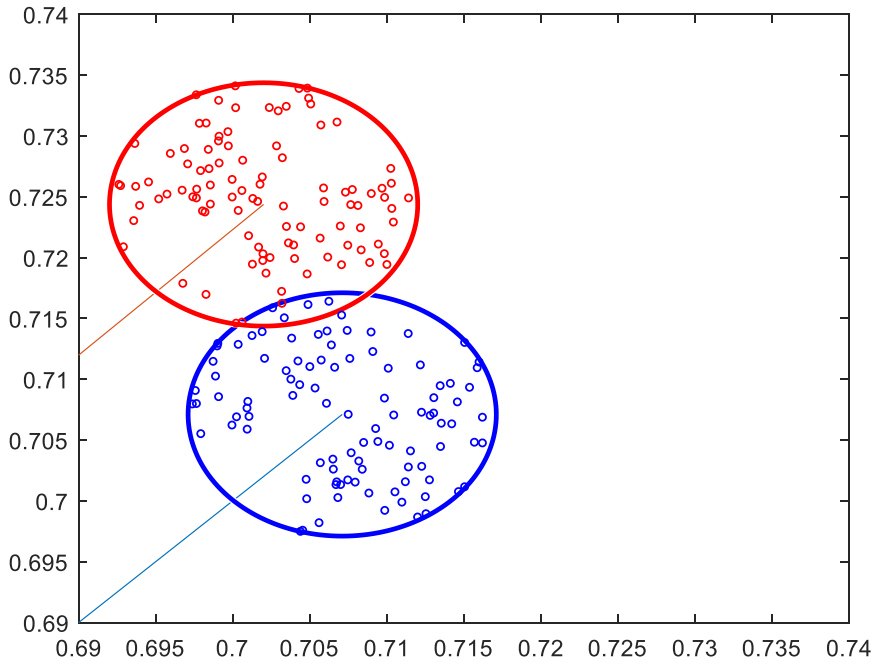

Figure 20. Possible estimates for a single vector pair.

The intrinsic error is most prevalent when subtraction operations are conducted on PMU phasor data. As such, a vector subtraction will be tested in this analysis. For each vector pair, n, the initial vector parameters, V_n^1 and V_n^2, are recorded. The difference vector, ΔV_n, for each of these initial vectors is also calculated as in equation (3.8).

$$\Delta V_n = V_n^1 - V_n^2 \tag{3.8}$$

Next, for each vector pair, n, an i number of estimate pairs, $V_{n,i}^1$, and $V_{n,i}^2$, are created within the respective TVE boundaries. These estimates are used to calculate an i number of normalized difference vectors, $\Delta V_{n,i}$, as shown in equation (3.9).

$$\Delta V_{n,i} = \frac{|V_{n,i}^1 - V_{n,i}^2|}{|\Delta V_n|} \tag{3.9}$$

The effect of TVE based intrinsic error can be visualized by plotting the variation of the calculated normalized difference vectors, obtained using the vectors estimated in presence of TVE, against the difference vectors calculated using the initial vector pairs. Figure 21. showcases the intrinsic error introduced by the simple subtraction operation. In particular, when the magnitude difference in the initial vectors is small, there exists a large variation in difference vectors calculated using the estimated vectors. As the magnitude difference in the initial vectors is increased, this variation diminishes and eventually converges to 1. This indicates minimal variation between the difference vectors. This observation, shown in Figure 21, is the basis for the claim that these higher variations occur when the difference between the 2 vectors being operated on is small and vice versa.

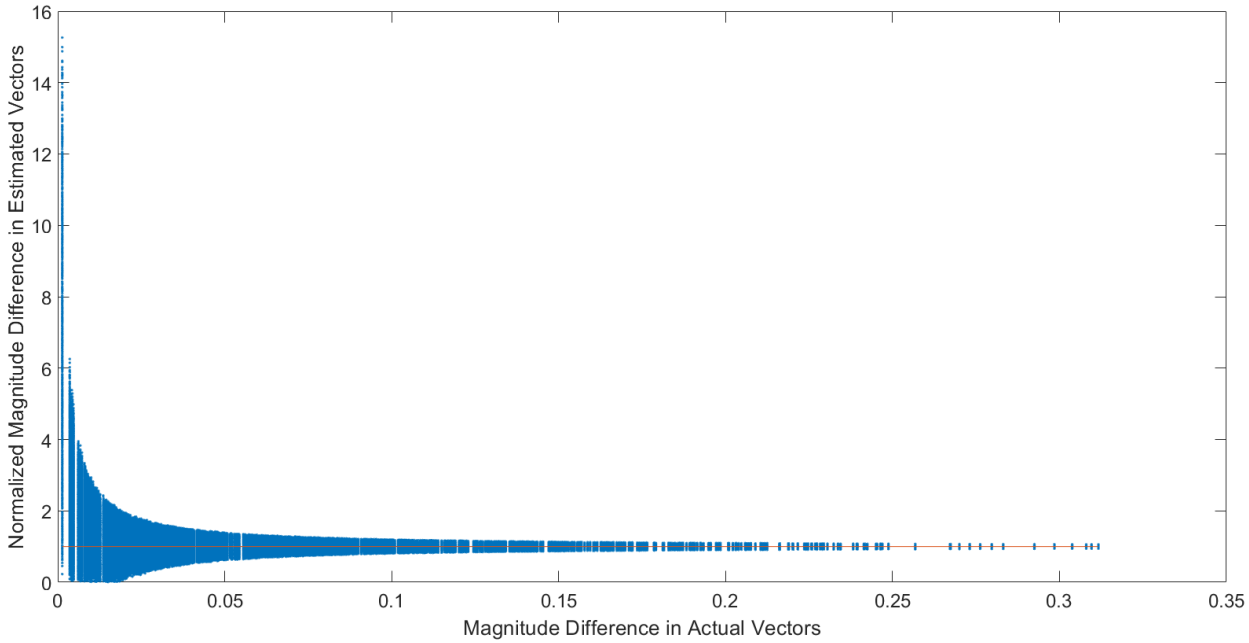

Figure 21. Relation between magnitude difference in actual vectors and the variation seen between their estimates.

CHAPTER 4

MODELING OF CORRECTION ALGORITHM

The resistance correction algorithm proposed in this work takes into account the variability of resistance estimations due to TVE and employees a 2 step approach to provide accurate estimations of resistance in near-real-time. The algorithm consists of a Recursive Decoupled Minimization (RDM) approach that is capable of working with complex values as those seen with PMU measurements. Also employed is an Artificial Neural Network (ANN) based correction portion which enables the algorithm to intelligently produce the best guess estimates for resistance based on dynamic real time system conditions. Overall, the proposed algorithm is able to output significantly accurate resistance estimations compared to the direct calculations based on raw PMU measurements as evidenced in Chapter 5.

The process initializes by obtaining the up-to-date current and voltage phasor measurements from the PMUs at either end of the transmission line in question. This would be $V_{s,i}^{m}$ and $I_{s,i}^{m}$ for the voltage and current respectively from the sending end PMU and $V_{r,i}^{m}$ and $I_{r,i}^{m}$ for the voltage and current respectively from the receiving end PMU at time i. However, these measurements are not used to directly calculate the line resistance as would be possible using the medium line model.

An RDM approach is then used to obtain corrected values of line resistance. This method is detailed in the following section. This corrected resistance estimate is then used in an Artificial Neural Network (ANN) based correction approach as detailed in section 4.2 . This takes into account a range of dynamic system parameters and uses a pre-trained ANN model to deduce the influence of these parameters in the determination of the final estimation of resistance.

4.1 Recursive Decoupled Minimization Algorithm

Traditional minimization approaches do not work well when the elements involved are in complex form [61]. Since this is the case here, a recursive decoupled minimization approach is used. This method allows the real and imaginary components of the objective function as well as the constraints to be worked on individually one after the other. In this particular case, after a solution is obtained, the variables are combined back into the complex form to check whether the overall objective is being achieved. The method is recursive because this process is repeated multiple times with the real and imaginary parts of the variable being worked on one after the other. Whenever the real part is considered as the variable, the imaginary part is treated as a constant and vice versa. Other than this, the minimization follows a standard Karush-Kuhn-Tucker (KKT) approach to minimization with inequalities [62].

The context behind the minimization approach is the vector difference observed between the two values of receiving end current available. The first current value is the receiving end current measurement obtained directly from the PMU, I_r^m. The other current value is an estimate, I_r^e, obtained using other system parameters as detailed below. The overall objective, therefore, is as written as in (4.1)

$$\min_{x,y}[(I_r^e(x,y) - I_r^m)^2] \tag{4.1}$$

$I_r^e(x,y)$, is the estimated receiving end current in terms of variables x and y where, x, is the real part of the estimated receiving end voltage and, y, is the imaginary part of estimated receiving end voltage. The estimated receiving end voltage, V_r^e, is used to calculate I_r^e as shown in equation (4.2) [42].

$$I_r^e = -\left[\frac{(V_r^e - V_s^m)}{Z^s} + \frac{(V_r^e \times Y^s)}{2}\right] \tag{4.2}$$

where,

$$Z^s = R + jX \tag{4.3}$$

$$Y^s = jB \tag{4.4}$$

R^s, X^s and B^s are the construction model resistance, reactance, and susceptance, respectively, for the particular line being investigated. V_s^m is the sending end voltage measured by the PMU. All terms are detailed in rectangular form as shown in Table 6.

TABLE 6

MINIMIZATION TERMS IN RECTANGULAR FORM

Term	Complex Term	Rectangular From
Estimated receiving end voltage	V_r^e	$x + j\ y$
Measured sending end voltage	V_s^m	$a + j\ b$
Construction model impedance	Z^s	$R + jX$
Construction model admittance	Y^s	jB
Measured receiving end voltage	V_r^m	$w_1 + jw_2$
Measured receiving end current	I_r^m	$p + jq$

The rectangular forms in Table 6 are substituted in equation (4.2) as to get.

$$I_r^e = -\left[\frac{((x+j\ y)-(a+j\ b))}{R+j\ X} + \frac{((x+j\ y)*jB)}{2}\right] \tag{4.5}$$

which would be expanded as shown in equation (4.6).

$$I_r^e = \left[\frac{x(-2R)+y(-2X+R^2B+X^2B)+(2Ra+2Xb)+j\left(x(2X-R^2B-X^2B)+y(-2R)+(2Rb-2Xa)\right)}{2R^2+2X^2}\right] \tag{4.6}$$

The objective from equation (4.1) would then be rewritten in expanded form as shown in equation (4.7).

$$\frac{x(-2R)+y(-2X+R^2B+X^2B)+(2Ra+2Xb-p)+j\left(x(2X-R^2B-X^2B)+y(-2R)+(2Rb-2Xa-q)\right)}{2R^2+2X^2} \tag{4.7}$$

To simplify equation (4.7), the constants and coefficients of the equation would be represented by the terms given in Table 7.

TABLE 7

REPRESENTATION OF CONSTANTS AND COEFFICIENTS

Representation	**Term**	**Full form**
Constant terms in real part	c_1	$2Ra + 2Xb - p$
Coefficient of x in real part	C_{x_r}	$-2R$
Coefficient of y in real part	C_{y_r}	$-2X + R^2B + X^2B$
Constant terms in imaginary part	c_2	$2Rb - 2Xa - q$
Coefficient of x in imaginary part	C_{x_i}	$2X - R^2B - X^2B$
Coefficient of y in imaginary part	C_{y_i}	$-2R$

After simplification, equation (4.7) can be written as shown in equation (4.8) and expanded as equation (4.9).

$$\min_{x,y}(I_e^R - I_m^R)^2 = \min_{x,y}\left[\frac{x*C_{x_r}+y*C_{y_r}+c_1+j\left(x*C_{x_i}+y*C_{y_i}+c_2\right)}{2R^2+2X^2}\right]^2 \tag{4.8}$$

$$\min_{x,y}(I_e^R - I_m^R)^2 = \min_{x,y}\left[\frac{\left(x*C_{x_r}+y*C_{y_r}+c_1\right)^2-\left(x*C_{x_i}+y*C_{y_i}+c_2\right)^2+2j\left(\left(x*C_{x_r}+y*C_{y_r}+c_1\right)*\left(x*C_{x_i}+y*C_{y_i}+c_2\right)\right)}{4R^4+4X^4+8R^2X^2}\right] \tag{4.9}$$

The objective would then split into its real and imaginary forms to supplement the RDM approach. In the case of the real part, equation (4.10) is obtained. $\tilde{y}$ is now a constant.

$$\min_{x}\left[\frac{\left(x^2\left(C_{x_r}{}^2-C_{x_i}{}^2\right)+\tilde{y}^2\left(C_{y_r}{}^2-C_{y_i}{}^2\right)+\left(c_1^2-c_2^2\right)+x\tilde{y}\left(2C_{x_r}C_{y_r}-2C_{x_i}C_{y_i}\right)+x\left(2C_{x_r}c_1-2C_{x_i}c_2\right)+\tilde{y}\left(2C_{y_r}c_1-2C_{y_i}c_2\right)\right)}{4R^4+4X^4+8R^2X^2}\right] \tag{4.10}$$

Equation (4.10) can be further simplified as shown in equation (4.11).

$$\min_{x}F_R = \left(x^2(A) + \tilde{y}^2(E) + (P) + x\tilde{y}(D) + x(K) + \tilde{y}(M)\right) \tag{4.11}$$

where,

$$A = \frac{{C_{x_r}}^2 - {C_{x_i}}^2}{4R^4+4X^4+8R^2X^2} \tag{4.12}$$

$$E = \frac{{C_{y_r}}^2 - {C_{y_i}}^2}{4R^4+4X^4+8R^2X^2} \tag{4.13}$$

$$D = \frac{2C_{x_r}C_{y_r} - 2C_{x_i}C_{y_i}}{4R^4+4X^4+8R^2X^2} \tag{4.14}$$

$$K = \frac{2C_{x_r}c_1 - 2C_{x_i}c_2}{4R^4+4X^4+8R^2X^2} \tag{4.15}$$

$$M = \frac{2C_{y_r}c_1 - 2C_{y_i}c_2}{4R^4+4X^4+8R^2X^2} \tag{4.16}$$

$$P = \frac{(c_1^2 - c_2^2)}{4R^4+4X^4+8R^2X^2} \tag{4.17}$$

As for the imaginary part, equation (4.18) is obtained. $\tilde{x}$ is now a constant.

$$\min_y \left[\frac{\left(\tilde{x}^2\left(2C_{x_r}C_{x_i}\right) + y^2\left(2\,C_{y_r}C_{y_i}\right) + \tilde{x}y\left(2C_{x_r}C_{y_i} + 2C_{y_r}C_{x_i}\right) + \tilde{x}\left(2C_{x_r}c_2 + 2C_1C_{x_i}\right) + y\left(2C_iC_{y_i} + 2C_2C_{y_r}\right) + c_1c_2\right)}{4R^4+4X^4+8R^2X^2} \right] \tag{4.18}$$

Equation (4.18) can be further simplified as shown in equation (4.19).

$$\min_y F_I = \left(\tilde{x}^2(S) + y^2(T) + (N) + \tilde{x}y(U) + \tilde{x}(V) + y(W)\right) \tag{4.19}$$

where,

$$S = \frac{2C_{x_r}C_{x_i}}{4R^4+4X^4+8R^2X^2} \tag{4.20}$$

$$T = \frac{2\,C_{y_r}C_{y_i}}{4R^4+4X^4+8R^2X^2} \tag{4.21}$$

$$U = \frac{2C_{x_r}C_{y_i} + 2C_{y_r}C_{x_i}}{4R^4+4X^4+8R^2X^2} \tag{4.22}$$

$$V = \frac{2C_{x_r}c_2 + 2C_1C_{x_i}}{4R^4+4X^4+8R^2X^2} \tag{4.23}$$

$$W = \frac{2C_iC_{y_i} + 2C_2C_{y_r}}{4R^4+4X^4+8R^2X^2} \tag{4.24}$$

$$N = \frac{c_1c_2}{4R^4+4X^4+8R^2X^2} \tag{4.25}$$

The constraint on the system is derived from the limitations set by TVE specifications in the IEEE Standard [8]. In line with the standard, the permissible error between the actual receiving

end voltage of the system being estimated, V_r^e, and the receiving end voltage measured by the PMU must be within 1%. Thus, a constraint is set as shown in equation (4.26).

$$(V_r^e - V_r^m)^2 \leq \left(\frac{V_r^m}{100}\right)^2 \tag{4.26}$$

The constraint is also expanded and decoupled as shown in equation (4.27).

$$x^2 - 2w_1x + w_1^2 - y^2 + 2w_2y - w_2^2 + 2j(xy - w_2x - w_1y + w_1w_2) \leq \frac{w_1^2 - w_2^2 + j2w_2}{100^2} \tag{4.27}$$

The real part being, with $\tilde{y}$ as a constant.

$$x^2 - 2w_1x + w_1^2 - \tilde{y}^2 + 2w_2\tilde{y} - w_2^2 \leq \frac{w_1^2 - w_2^2}{100^2} \tag{4.28}$$

$$G_R = x^2 - 2w_1x + w_1^2 - \tilde{y}^2 + 2w_2\tilde{y} - w_2^2 - \frac{w_1^2 - w_2^2}{100^2} \leq 0 \tag{4.29}$$

and the imaginary part being, with $\tilde{x}$ as a constant.

$$\tilde{x}y - w_2\tilde{x} - w_1y + w_1w_2 \leq \frac{w_2}{100^2} \tag{4.30}$$

$$G_I = \tilde{x}y - w_2\tilde{x} - w_1y + w_1w_2 - \frac{w_2}{100^2} \leq 0 \tag{4.31}$$

The RDM process consists of 2 decoupled minimization processes. First is the real objective, $\min_x F_{real}$, and associated constraint, G_{real} This is worked on with the real part of the initial variable, x, being treated as the variable being solved for. During this stage, the imaginary part of the initial variable, y, is treated as a constant, $\tilde{y}$. The other process is the imaginary objective, $\min_y F_{imag}$, and associated constraint, G_{imag}, of the problem. Here, the imaginary part of the initial variable, y, is treated as a variable while the real counterpart, x, newly changed or otherwise, is treated as a constant, $\tilde{x}$. An intermediate error checking process detailed next is run after each part and the new solution is retained or discarded accordingly.

The intermediate error checking process ensures that the RDM process only continues while it is able to continuously minimize the error between the measure and estimated receiving

end current after each minimization step. When the algorithm detects that the error is no longer reducing, the RDM process is terminated.

It is possible for the process to terminate without finding a solution to either part of the minimization. Since the system is designed to work on real data with the possibility of consisting highly erratic outliers, such cases would be handled this way as it would not be possible for the algorithm to find solutions while adhering to the set constraints. Such issues are later dealt with during the ANN correction step.

At the conclusion of the RDM process, corrected values of line resistance, R^c, and the resulting sending end current estimate, I_s^e, are found as shown in equations (4.32) and (4.33).

$$R^c = \Re\left[\frac{{V_{s,i}^e}^2 - {V_{r,i}^e}^2}{V_{s,i}^e I_{r,i}^e + V_{r,i}^e I_{s,i}^e}\right] \tag{4.32}$$

$$I_s^e = \frac{V_s^m - V_r^e}{(R^c + jX)} + \frac{V_s^m \times Y^c}{2} \tag{4.33}$$

Considering the 2 minimization processes in the RDM algorithm, each being a constrained minimization with inequality constraints, a Karush-Kuhn-Tucker (KKT) based approach would be employed. Thus, the first order necessary conditions, shown in equation (4.34), (4.35) and (4.36), must be met for a solution to exist [63].

$$\mu^* \geq 0 \tag{4.34}$$

$$\nabla f(x^*) + {\lambda^*}^T \nabla h(x^*) + {\mu^*}^T \nabla g(x^*) = 0 \tag{4.35}$$

$${\mu^*}^T \nabla g(x^*) = 0 \tag{4.36}$$

Where f, h and g are continuously differentiable objective function, equality constraint and inequality constraint, respectively. x^*would be the local minimum of the objective, f, subject to $h(x) = 0$ and $g(x) \leq 0$ where $\lambda \in \mathbb{R}$ and $\mu \in \mathbb{R}$. λ is the Lagrange multiplier and μ, the KKT multiplier. The problem presented in this work would not contain an equality constraint.

Therefore, in the case of the real part, the objective function given in equation (4.11) and constraint equation (4.29) would form the Lagrangian function, $\mathcal{L}_R(x, \mu_R)$.

$$\mathcal{L}_R(x, \mu_R) = x^2(A) + \tilde{y}^2\ (E) + (P) + x\tilde{y}(D) + x(K) + \tilde{y}(M) + \mu_R(G_R) \tag{4.37}$$

The differential of which would produce

$$\nabla_x \mathcal{L}_R(x, \mu_R) = 2Ax + D\tilde{y} + K + \mu(2x - 2w_1) = 0 \tag{4.38}$$

The condition, $\mu^{*T} \nabla g(x^*) = 0$, must also be met as shown in equation (4.39).

$$\mu_R \left(x^2 - 2w_1 x + w_1^2 - \tilde{y}^2 + 2w_2\tilde{y} - w_2^2 - \frac{w_1^2 - w_2^2}{100^2}\right) = 0 \tag{4.39}$$

Therefore, 2 scenarios would be considered as shown in Table 8.

TABLE 8

SOLUTION AND FEASIBILTY OF REAL PART MINIMIZATION

	Scenarios to consider	
KKT multiplier	$\mu_R = 0$	$\mu_R \neq 0$
Solution	$x^* = \dfrac{-K - D\tilde{y}}{2A}$	$x^* = \dfrac{2\mu_R w_1 - K - D\tilde{y}}{2A + 2\mu_R}$
Feasibility	$\mu_R^* = 0$ $\mu_R^* \nabla G_R(x^*) = 0$ $\nabla_x \mathcal{L}_R(x^*, \mu_R) = 0$	$\mu_R^* > 0$ $\nabla G_R(x^*) = 0$ $\nabla_x \mathcal{L}_R(x^*, \mu_R) = 0$

In the case of the imaginary part, the objective function given in equation (4.19) and constraint equation (4.31) would form the Lagrangian function, $\mathcal{L}_I(y, \mu_I)$.

$$\mathcal{L}_I(y, \mu_I) = \tilde{x}^2(S) + y^2(T) + (N) + \tilde{x}y(U) + \tilde{x}(V) + y(W) + \mu_I(G_I) \tag{4.40}$$

The differential of which would produce

$$\nabla_y \mathcal{L}_I(y, \mu_I) = 2Ty + U\tilde{x} + W + \mu_I(-w_1 + \tilde{x}) = 0 \tag{4.41}$$

The condition, $\mu^{*T} \nabla g(x^*) = 0$, must also be met as shown in equation (4.42).

$$\mu_I \left(\tilde{x}y - w_2\tilde{x} - w_1 y + w_1 w_2 - \frac{w_2}{100^2} \right) = 0 \tag{4.42}$$

Therefore, 2 scenarios would be considered as shown in Table 9.

TABLE 9

SOLUTION AND FEASIBILTY OF IMAGINARY PART MINIMIZATION

	Scenarios to consider	
KKT multiplier	$\mu_I = 0$	$\mu_I \neq 0$
Solution	$y^* = \frac{-W - U\tilde{\mathrm{x}}}{2T}$	$y^* = \frac{\mu_I w_1 - \mu_I \tilde{\mathrm{x}} - U\tilde{\mathrm{x}} - W}{2T}$
Feasibility	$\mu_I^* = 0$ $\mu_I^* \nabla G_I(y^*) = 0$ $\nabla_y \mathcal{L}_I(y^*, \mu_I) = 0$	$\mu_I^* > 0$ $\nabla G_I(y^*) = 0$ $\nabla_y \mathcal{L}_I(y^*, \mu_I) = 0$

At each minimization step, the values of the constants would determine the feasibility of each scenario in both the real and imaginary parts and apply the solution accordingly. This solution is then pushed through the intermediate checking phase. The overall process is detailed in Figure 22.

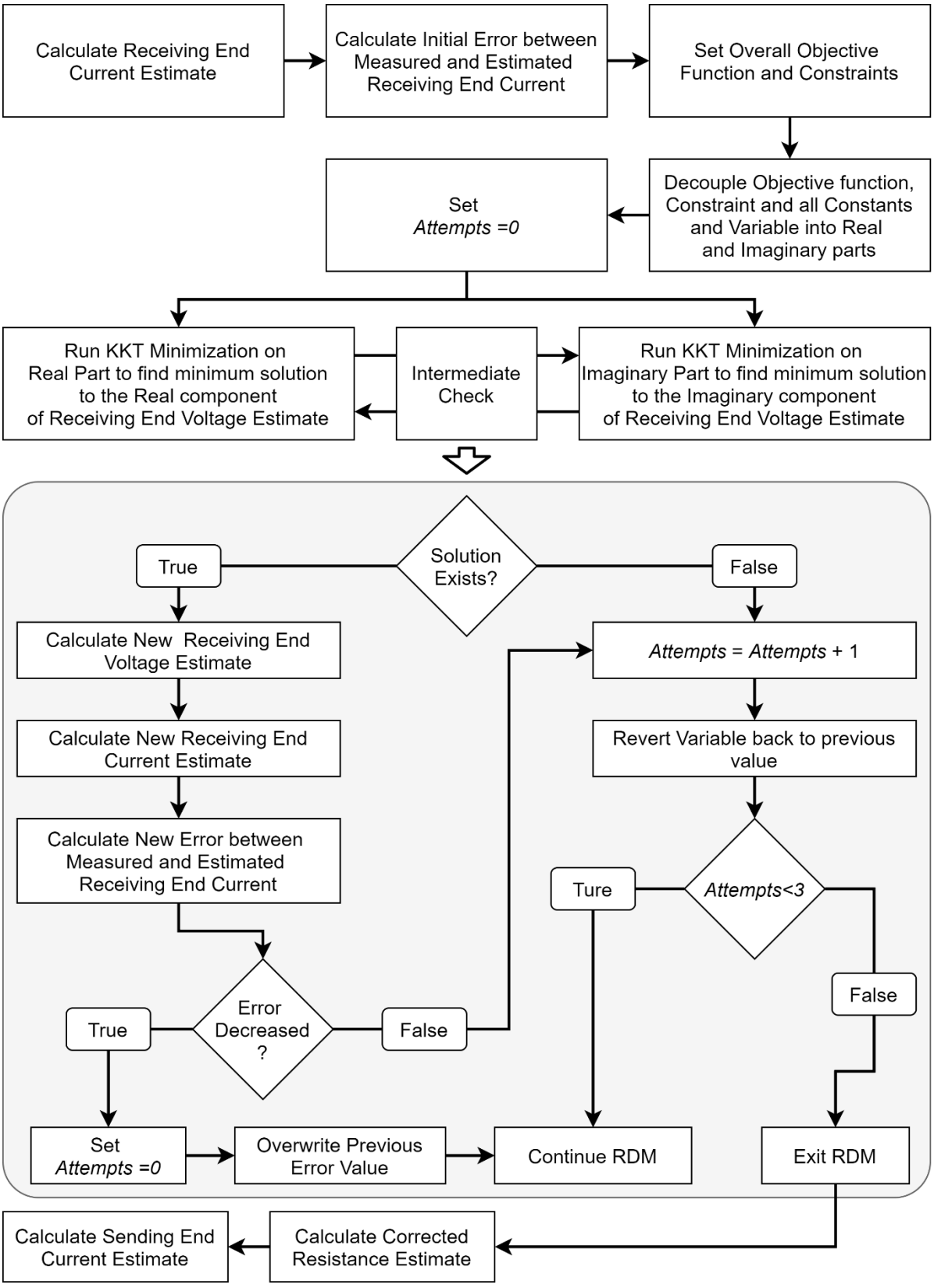

Figure 22. Recursive decoupled minimization process.

4.2 Artificial Neural Network Based Correction

In depth simulation and analysis of system behavior in the presence of TVE laden data show the existence of distinct correlations between the error in resistance estimations and certain instantaneous system parameters. The most notable of these, as mentioned earlier, is the higher possibility of error when the line loading is low. As shown is Figure 23, although a drastic improvement in comparison to the error seen against the direct estimation of resistance, as shown in Figure 14, there still exists a significant percentage of error particularly in the low line loading conditions. In the current state, the corrected resistance estimation would only be useful to a utility at very high line loading situations when the error falls within $\pm 10\%$. While this is still a significant advantage to utilities as the very high line loading situations are the most critical in terms of observability, additional system parameters were studied to find additional correlation factors to this error.

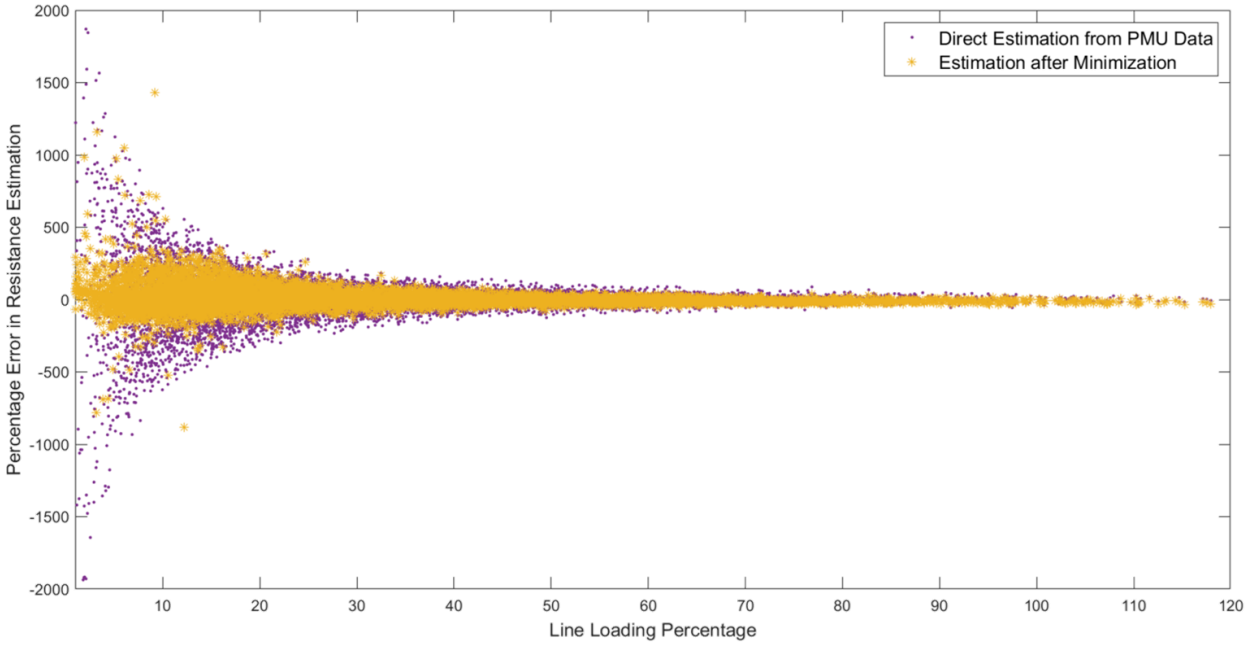

Figure 23. Percentage estimated resistance error against percentage line loading.

Another interesting find is the change in corrected resistance error with angle difference observed between the measured and estimated readings of receiving end current. This is shown in Figure 24. A similar, slightly less significant, correlation is found in the sending end counterpart.

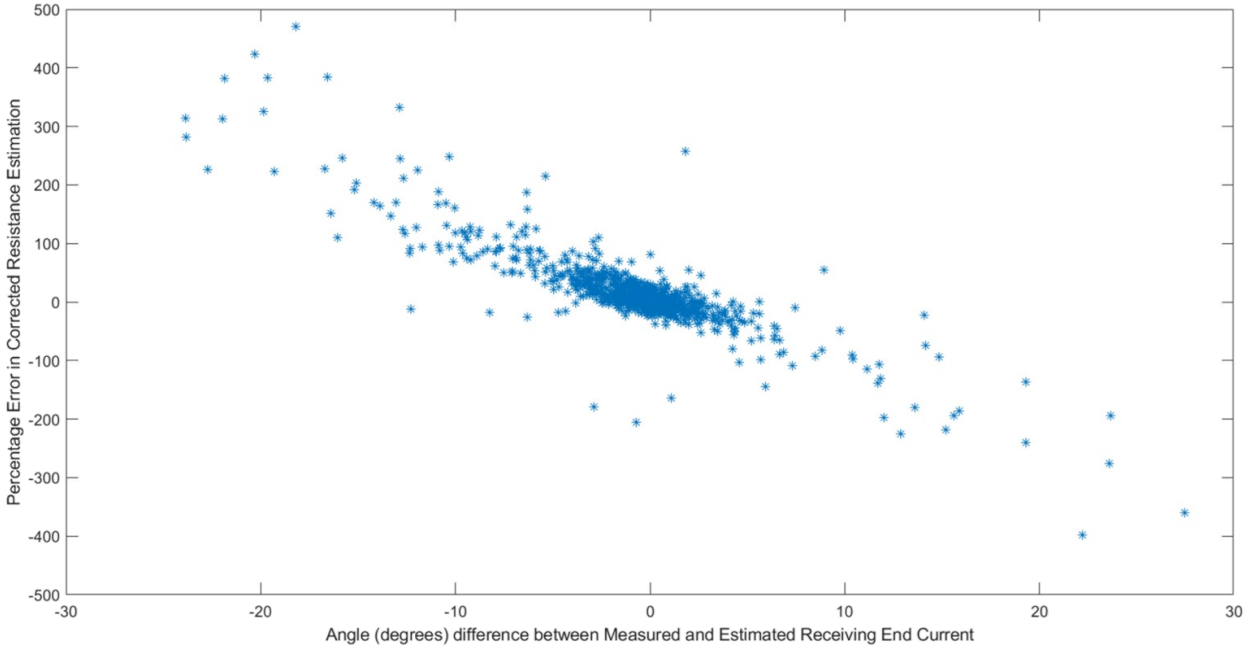

Figure 24. Percentage corrected resistance error against angle difference observed between the measured and estimated readings of receiving end current.

Another pattern is observed when the error in corrected resistance is plotted against the change in measure voltage angle between either end of the line as shown in Figure 25.

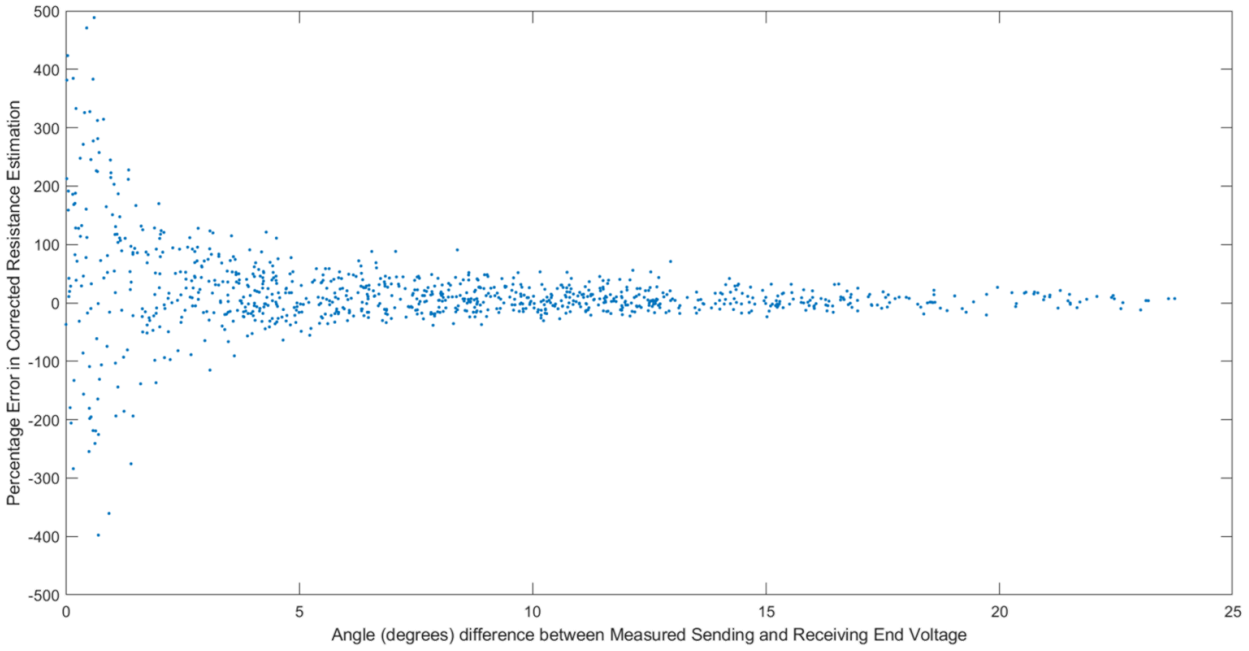

Figure 25. Percentage corrected resistance error against angle difference measured between the sending and receiving end voltage.

There also exists a significant correlation between the corrected resistance error and the deviation of the corrected resistance from the construction model resistance as shown in Figure 26. The figures used to demonstrate the existence of certain correlation were derived from various sets of data. The correlations however can be replicated and have been observed and studied in multiple transmission lines of varying lengths, current carrying capacities, geographic locations, and construction parameters. In addition to these system parameters, the change in magnitude of sending and receiving end currents as well as the measured drop in voltage across the line and the system frequency were also included in final ANN model creation. Using accurate simulations of each particular transmission line with simulated TVE, a set of ANN models, one per line, was created.

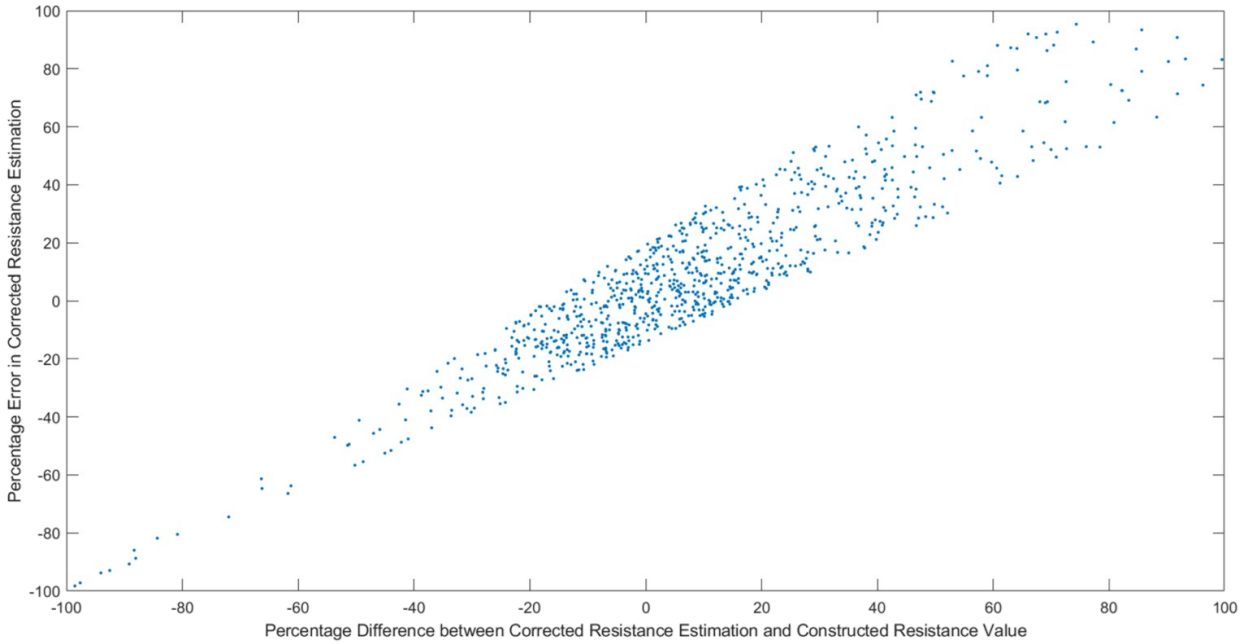

Figure 26. Percentage corrected resistance error against percentage difference between corrected resistance estimation and construction resistance value.

For ANN modeling, a Levenberg–Marquardt algorithm approach was used [64]. In the model creation step, the data was split, 70%, 15% and 15% for Training, Validation and Testing. 10 hidden neuron setup was used. The 15% of data used for validation is used to ensure that overfitting is prevented. The 15% of data maintained for testing is kept completely separate during the training and validation phases and only used to finally test the fit of the created model. The training continues until the error is no longer being reduced. For training each model, 1000 discontinuous data points were randomly selected. The selection included data from all times of the day, seasons of the year and system loading conditions. This variation in training data, representing the variations seen in the real world, allows the model to be capable of handling varying real world system conditions.

As mentioned earlier, 8 input parameters are used for the creation of the ANN correction model for each line as shown in Table 10Table 11. The output, or target, during model creation

was the deviation between the resistance estimation obtained from the minimization step earlier and the actual resistance simulated in the system. Therefore, in model application, a correction factor would be produced based on the inputs given.

TABLE 10

PARAMETERS FOR ANN CORRECTION

Inputs	
ΔI_s^{mag}	Magnitude difference between measured and estimated sending end current
ΔI_r^{mag}	Magnitude difference between measured and estimated receiving end current
ΔI_s^{angle}	Angle difference between measured and estimated sending end current
ΔI_r^{angle}	Angle difference between measured and estimated receiving end current
ΔV_{sr}^{angle}	Angle difference between sending and receiving end measured voltage
ΔV_{sr}^{mag}	Magnitude difference between sending and receiving end measured voltage
$Freq$	Instantaneous System Frequency
ΔR_{cs}	Deviation of corrected resistance estimation from conduction model value
Output	
ΔR_{ca}	Deviation of corrected resistance estimation from actual system value

The layout of the ANN model is as shown in Figure 27. W and B represent the weight and bias factors used for modeling respectively. Figure 28 shows the performance of a model for a particular line during training. To reach the minimum mean squared error, 399 iterations are run in this case. Figure 29 shows the histogram of encountered errors during this model creation process and Figure 30 shows the regression plots is each stage of the model creation process.

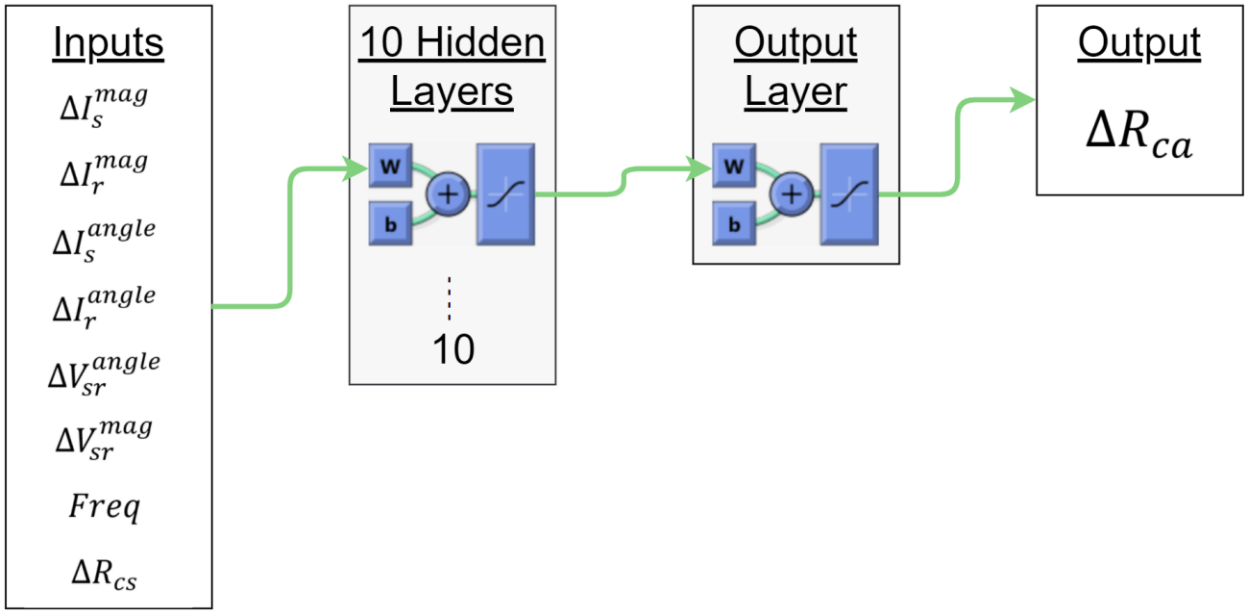

Figure 27. Model for Artificial Neural Network

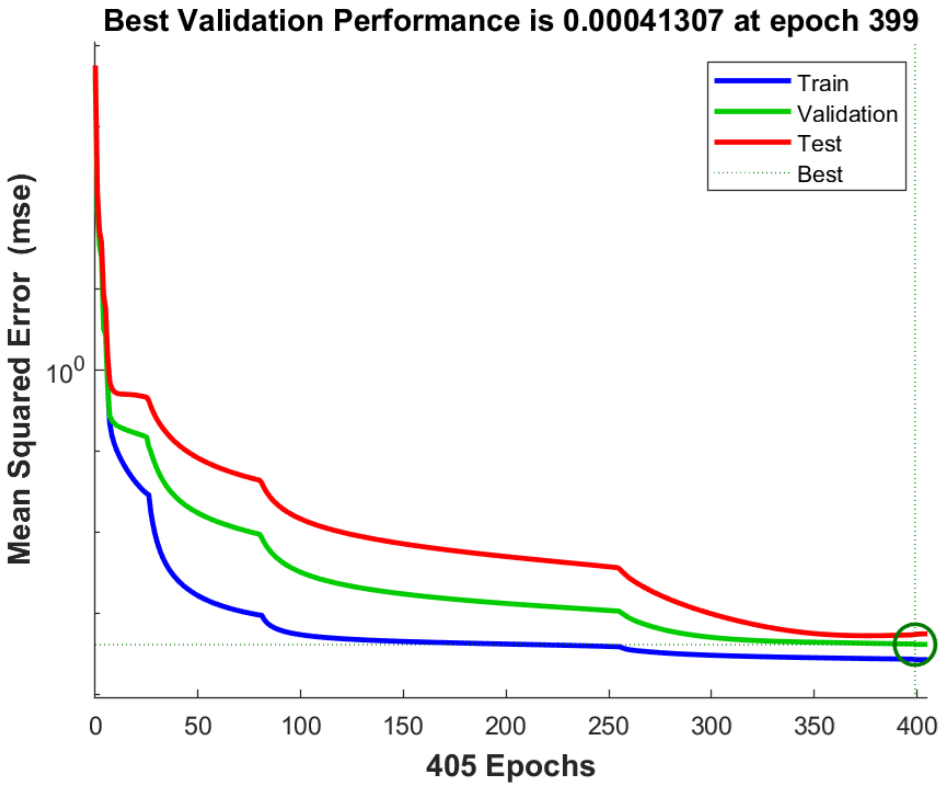

Figure 28. ANN performance during training

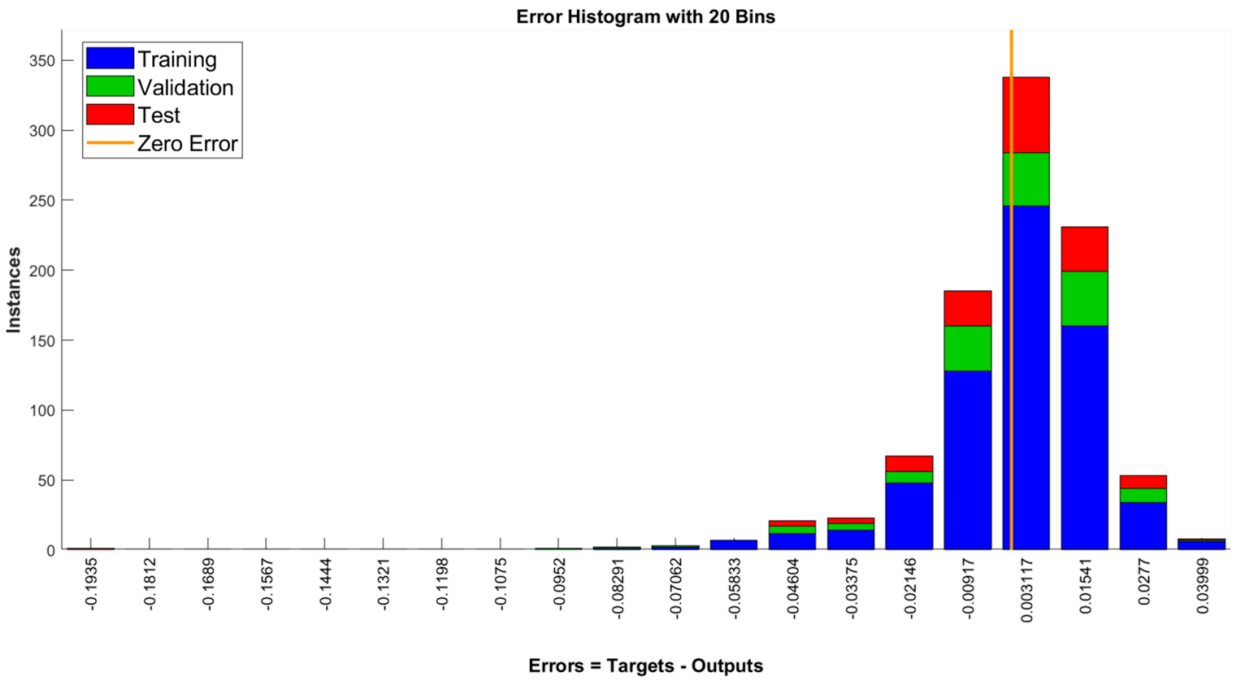

Figure 29. Histogram of errors during model training.

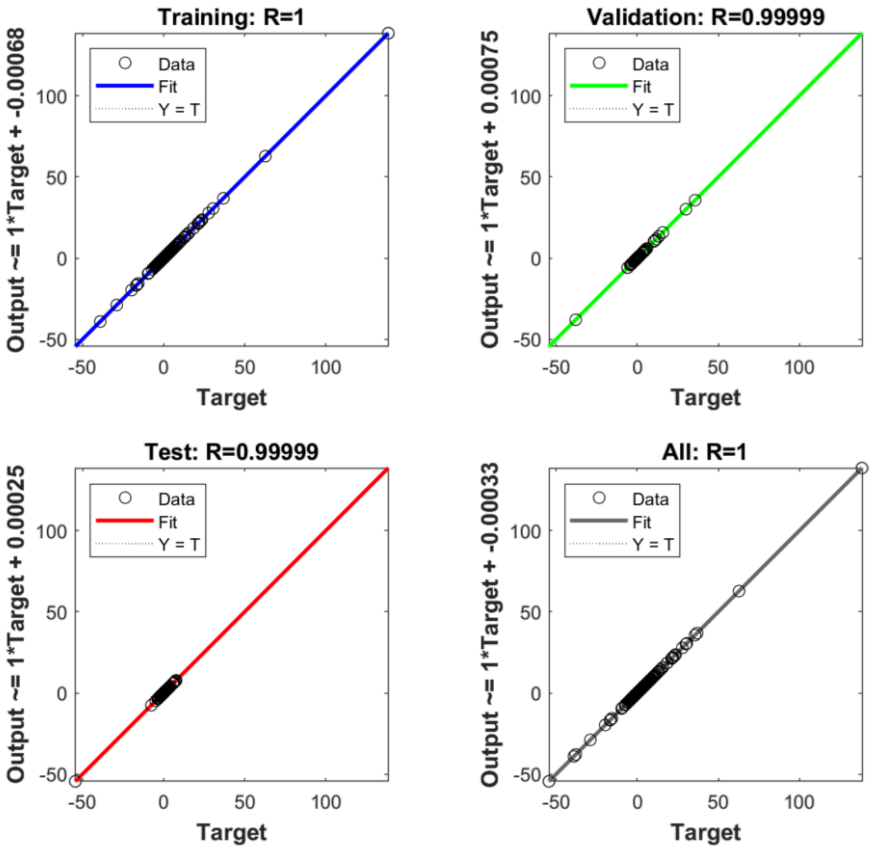

Figure 30. Regression plot from ANN model creation.

Once an ANN correction model is created and saved for each line, these models can then be used to produce dynamic correction factors in real time based on the instantaneous system parameters inputs mentioned in Table 10. The resulting correction factor output is then applied on the resistance estimation produced during the minimization step to obtain the final resistance estimations. As expected, the resulting final resistance estimations are capable of producing significantly less error as shown in Figure 31. The actual improvements seen will be analyzed in detail in Chapter 5. Thus, in real world application, an ANN model would be premade for each transmission line in the network and updates to this model would only be necessary if physical changes are made to the line.

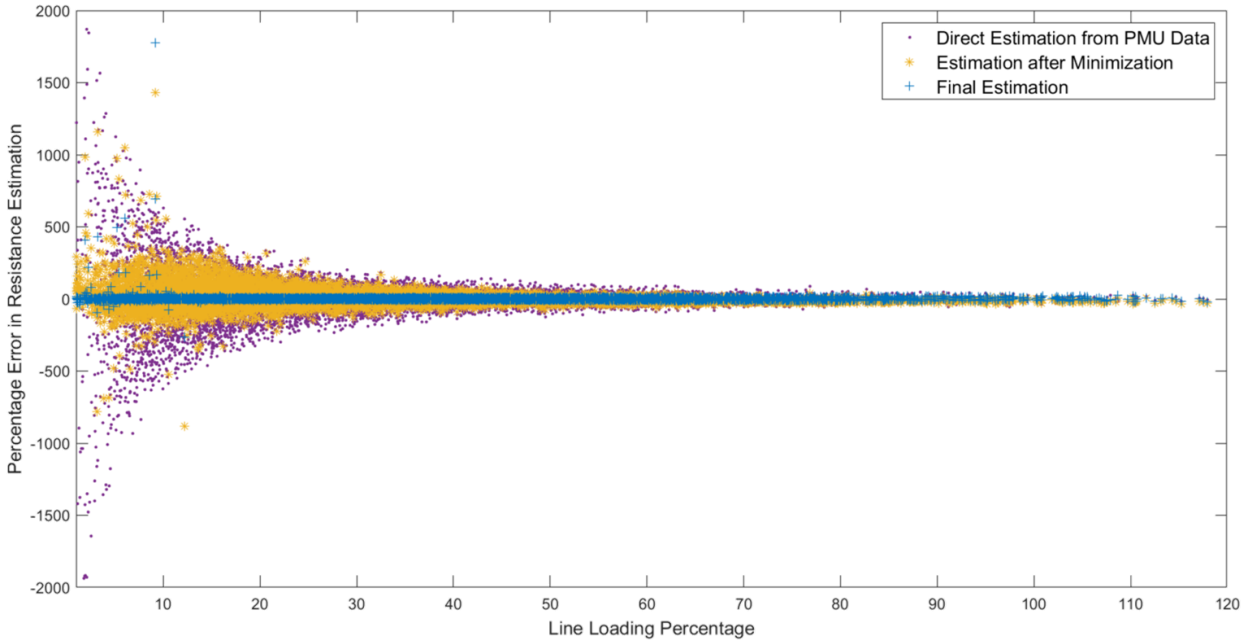

Figure 31. Percentage estimated resistance error against percentage line loading.

The complete outline of the resistance estimation and ANN based correction process is shown in Figure 32.

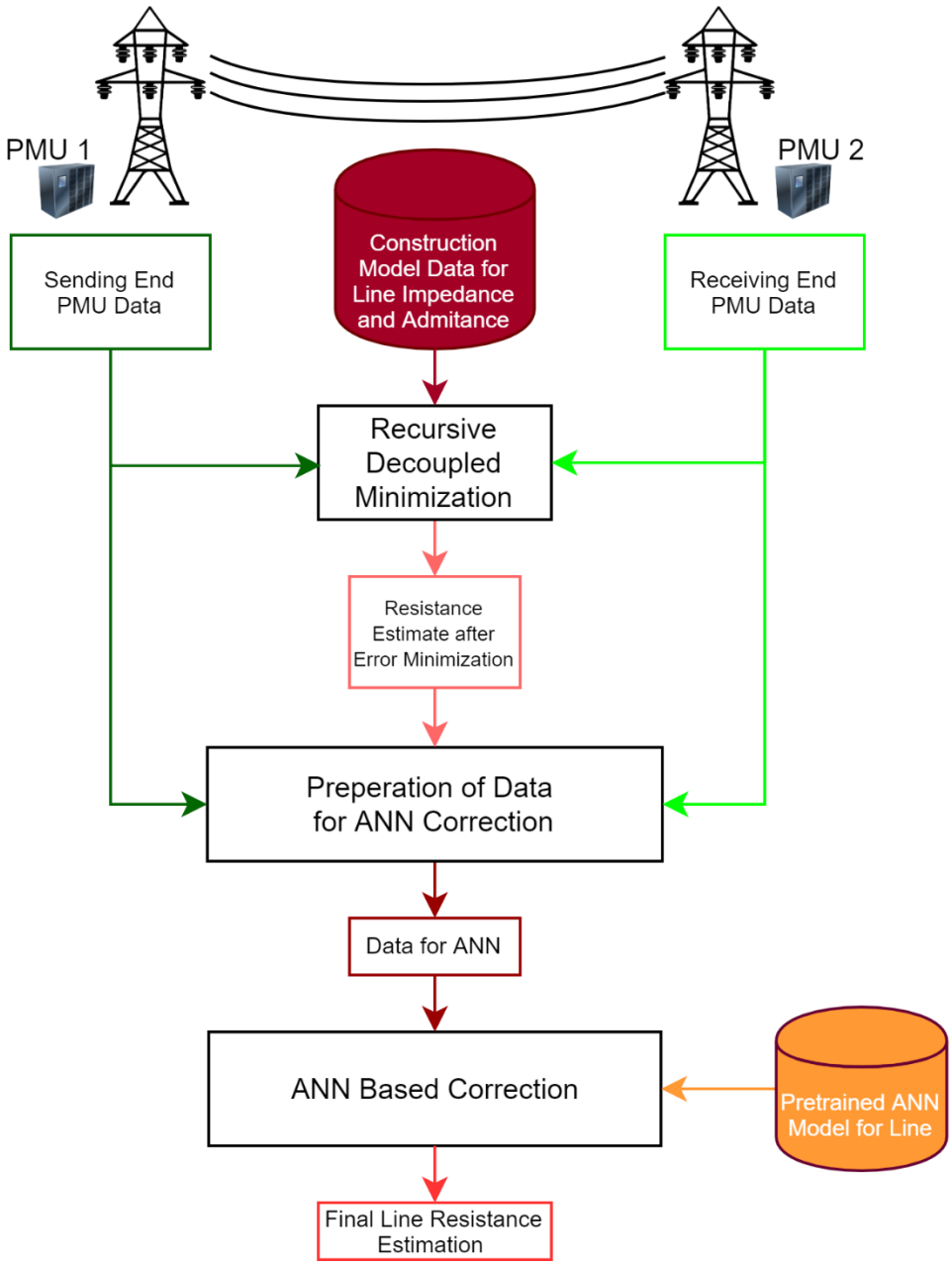

Figure 32. Process outline for the Proposed Correction Algorithm.

4.3 Application in Continuous Time

Since the correction algorithm does not rely on data aggregation or a moving window in application, the algorithm can be applied in real time or in synchronization with the data input into the system. As required, the algorithm can also be applied at a slower sampling rate than the PMU sampling rate data in order to save on computing power.

Figure 33 showcases the application of the complete algorithm in 1 minute of continuous data. The actual resistance simulated in the system is shown as are the resistance estimations done directly from the PMU measurements (Initial Estimation), the estimation after the error minimization step (Corrected Estimation) and the final estimation after the algorithm. The sampling rate of the data was set to that of the PMU data. This allows the rapid variation in the initial resistance estimation to be visible. However, the final estimation is largely unaffected. Figure 34 showcases the application of the algorithm in another 1 minute of continuous data at a sampling rate of 1 per second.

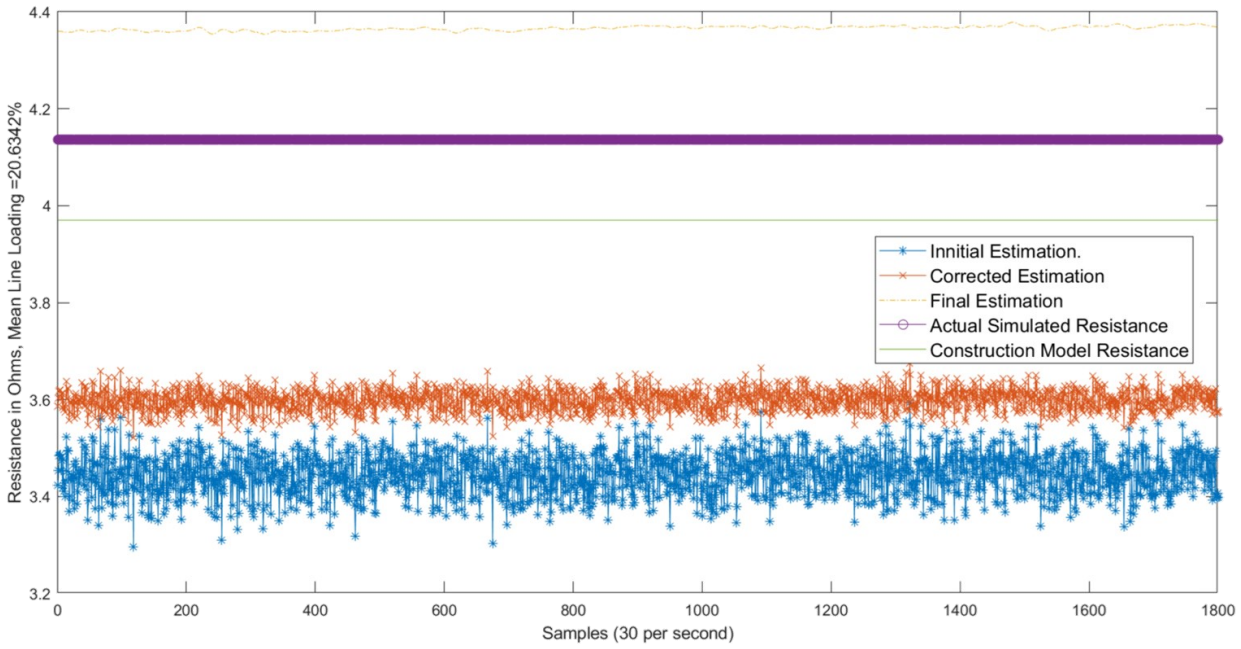

Figure 33. Continuous time application at PMU sampling rate.

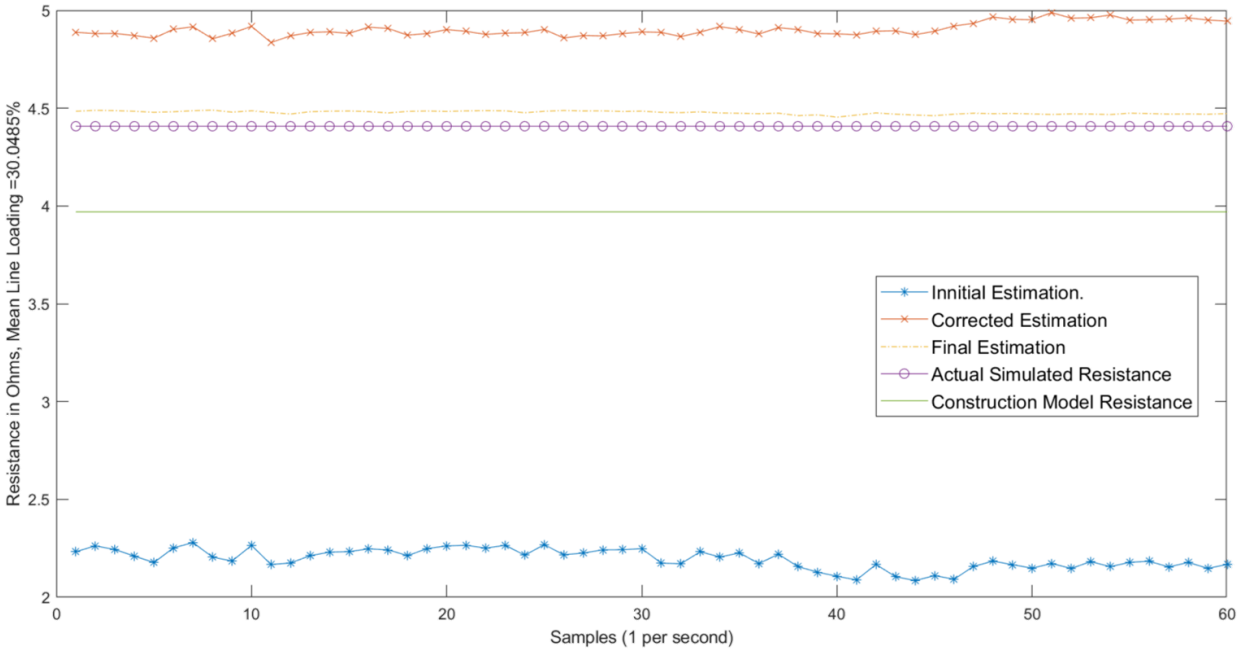

Figure 34. Continuous time application at reduced sampling rate.

Although missing and outlier data is a valid concern in real PMU data, for the purpose of this work, it is assumed that all data is available and errors present are due to the intrinsic noise and bias in PMU data and not outlier events.

CHAPTER 5

NUMERICAL ANALYSIS OF ALGORITHM

The performance of the transmission line resistance estimation correction algorithm proposed in this work was analyzed using real PMU data provided by a utility operating over 200 PMU devices on a state-wide network. The analysis was conducted under varying system conditions include times of the day, environmental conditions and changes in line loads and were conducted on transmission lines of varying lengths, conductor properties and construction parameters. The analysis included 2 modes.

Firstly, multiple lines were simulated with dynamic, yet known, resistances and mimicking real world system loads. The proposed algorithm was tested to gauge performance with both non-continues data inputs as well as time series continuous data flows. Second, the proposed algorithm was applied on real world PMU data with unknown actual resistance parameters. Here, only the construction model values for resistance are known. Yet, it is possible to ensure that the final estimations produced by the algorithm remain sensical in contrast to the initial estimations derived directly from the measured PMU data. Multiple lines were also tested in this manner.

5.1 Simulation Testing

The A virtual set up was created to simulate the effects TVE plays on the PMU derived readings. A single transmission line containing a PMU at either end was modeled. As per standard, these PMUs would provide voltage and current data as phasor measurements. The transmission line would have a fixed reactance, and susceptance, to match that of a real transmission line operated by the utility. These values would be obtained from the construction data for the line. The conductance was ignored for this analysis as its effect is minimal [4]. The actual line resistance of

the line, an unknown value in the real world, was varied to simulate the increase in line resistance due to heating, line loading and other factors.

A large set of data point representing varying times of the day, environmental conditions and system conditions was used for the 1st test. For testing purposes, 6 transmission lines, connected to 12 PMU devices, were selected. The selected lines represented variations in line lengths, current carrying capacities, conductor types as well as construction parameters as shown in TABLE 11. The initial resistance estimation, the estimation after error minimization as well as the final resistance estimation for each data point on each line was compared the actual instantaneous resistance of the line to obtain a percentage of error.

TABLE 11

TRANSMISSION LINE SELECTION FOR TESTING

Line Length (~Miles)	**Line Capacity (Amps)**	**Conductor Type**	**Base Voltage (kV)**	**Construction Model Resistance (Ω)**	**Construction Model Reactance (Ω)**
94.4	907	Drake	345	3.315	54.790
72.0	1607	Kiwi	345	3.970	53.704
62.0	907	Drake	345	3.981	36.416
20.3	907	Drake	345	1.311	12.277
20.1	1607	Kiwi	345	1.069	15.714
12.0	475	Partridge	138	4.556	9.915

Table 12 shows the resulting mean errors for each estimation. It also shows the significant reduction in estimation error across the board when comparing the initial estimation direct from the PMU measurements against the final estimation obtained through the proposed algorithm. The mean estimation error resulting from the final estimation remains below 10% for all the tested lines. Also of note, shorter lines with higher capacities performed the worst in the initial

estimations. This is in line with expectations based on the effect of TVE. Short lines however perform well under the proposed algorithm regardless of current capacity. There exists a distinct relationship between the mean error in final estimation and the length and capacity of the line. Plotting the capacity by length factor against the mean final estimation for each line, a relation is observable as shown in Figure 35. However, a comprehensive analysis with a large number of varied transmission lines would have to be conducted to conclude this hypothesis.

TABLE 12

MEAN ERROR, COMPARING RESISTANCE ESTIMATIONS

Line Length (~Miles)	**Line Capacity (Amps)**	**Mean Error Percentage**			**Capacity/ Length**
		Initial Estimation	**Corrected Estimation**	**Final Estimation**	
94.4	**907**	181.43 %	71.51 %	8.84 %	9.61
72.0	**1607**	109.91 %	45.74 %	2.39 %	22.57
62.0	**907**	92.89 %	36.90 %	7.63 %	14.63
20.3	**907**	206.71 %	79.17 %	4.71 %	44.68
20.1	**1607**	322.57 %	93.10 %	1.21 %	79.95
12.0	**475**	114.51 %	41.41 %	5.60 %	39.58

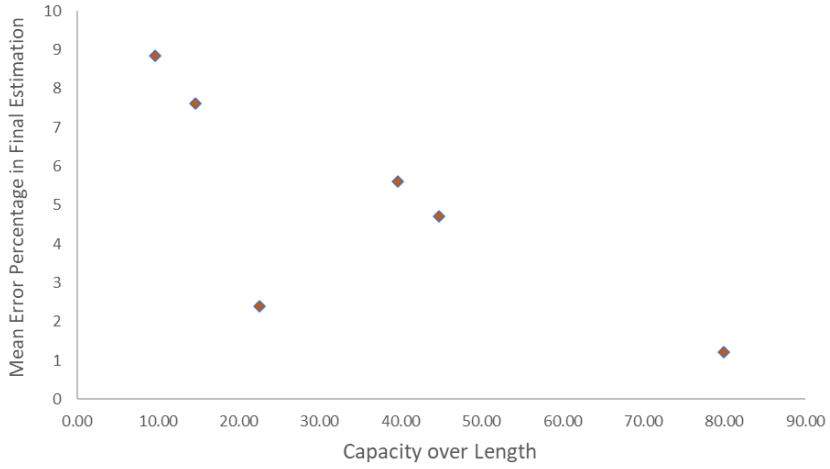

Figure 35. Plot of capacity over length against mean error in estimations.

The outlier point is a result of that particular line consistently running well below 30% of its capacity. This low utilization serves better than expected estimation results.

The lines were then tested to gauge the performance of the algorithm at varying line loading levels. Table 13 shows the resulting errors, both initial and final, on each line at varying line loading percentages. Redder colors represent worse error while a greener color indicate lesser error.

TABLE 13

ERROR CHANGE WITH LINE LOADING

Line Load Percentage	Line Length (~Miles)											
	12.0		20.1		20.3		62.0		71.2		94.4	
	Initial Error %	Final Error %	Initial Error %	Final Error %	Initial Error %	Final Error %	Initial Error %	Final Error %	Initial Error %	Final Error %	Initial Error %	Final Error %
<10%	438.3	15.4	1374.7	3.5	1942.1	20.9	489.3	7.4	371.4	2.1	1079.7	11.7
10%-20%	142.3	3.0	393.0	1.1	503.7	4.5	188.6	3.2	100.4	0.4	307.5	8.6
20%-30%	77.8	3.3	188.9	0.8	270.6	1.6	105.5	4.3	55.7	0.5	125.0	8.4
30%-40%	50.7	4.2	134.3	0.7	174.4	1.2	78.3	5.6	33.8	0.5	94.4	8.2
40%-50%	36.8	5.1	95.8	0.7	150.6	1.4	49.4	6.3	30.8	0.5	61.7	9.1
50%-60%	31.2	5.8	83.7	0.7	118.1	1.2	40.7	7.7	19.8	0.4	57.8	8.8
60%-70%	25.7	6.5	69.0	0.7	98.8	1.5	31.5	8.6	17.7	0.3	48.4	8.3
70%-80%	20.3	7.0	58.5	0.8	80.2	1.2	28.6	9.2	17.7	0.3	41.0	7.9
80%-90%	18.4	8.2	48.2	0.8	63.0	1.1	24.8	9.8	12.0	0.4	25.9	8.6
90%-100%	17.0	9.1	42.0	1.0	56.0	1.2	23.9	10.1	6.2	0.2	31.1	8.3
100%-110%	13.8	8.9	35.6	0.5	40.7	0.9	20.1	10.0	11.7	1.1	34.1	9.6
>110%	12.6	10.7	30.0	1.3	42.7	0.8	18.6	10.1	7.6	1.3	21.9	5.3

According to Table 13, the initial resistance error is very high for all lines under low loading conditions. This is as expected and observed. The final resistance also performs its worst under these conditions and sometimes edges past 10%. Both resistances improve as the line loading increases with the final estimation error dropping rapidly and initial resistance error dropping much slower. The performance of the final estimation error increases slightly as the line loading increases beyond 100% but still remains below that of the initial estimation.

The variation detailed above can be better visualized with a pair of box plot diagrams comparing the performance of each estimation. Figure 36 and Figure 37 showcases 2 medium length lines while Figure 38 and Figure 39 showcases 2 short length lines. The final resistance estimations consistently show a lesser percentage error in all cases.

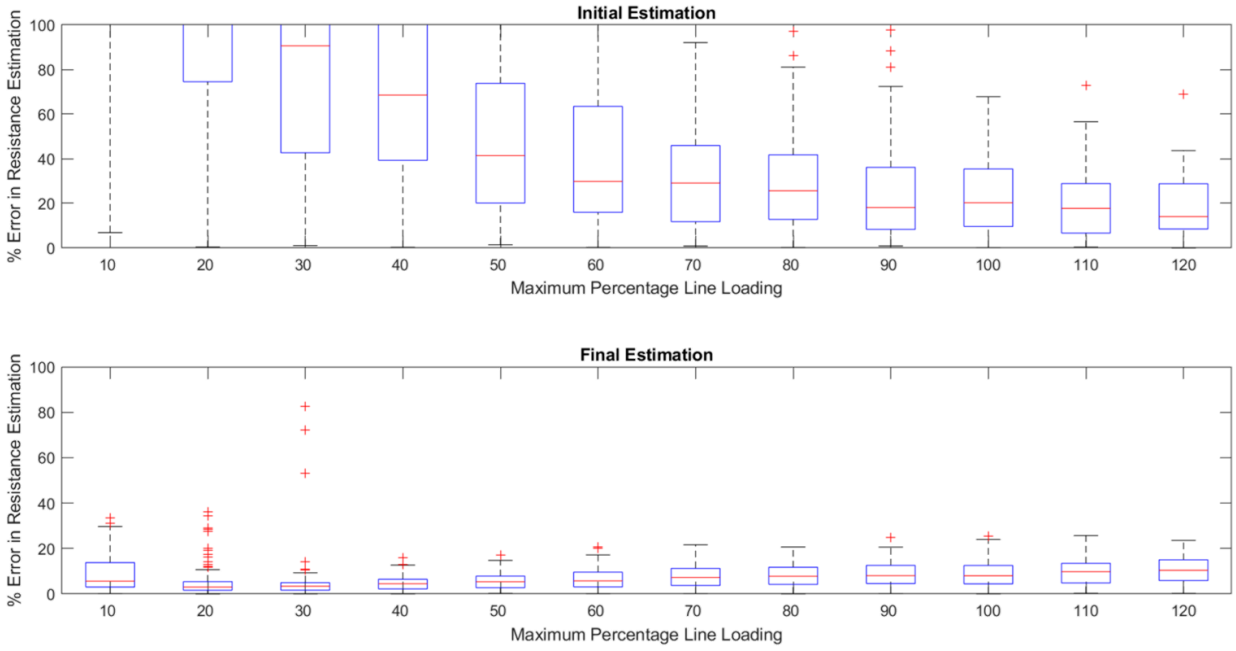

Figure 36. Box plot for error comparison, medium line 1.

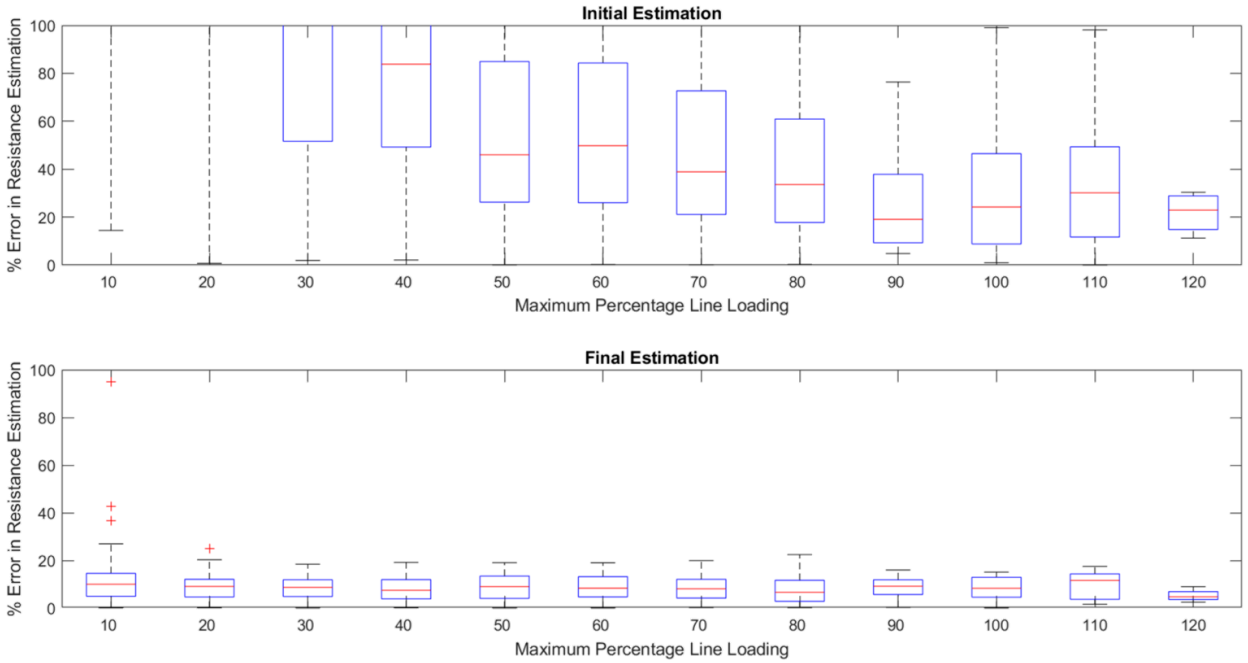

Figure 37. Box plot for error comparison, medium line 2.

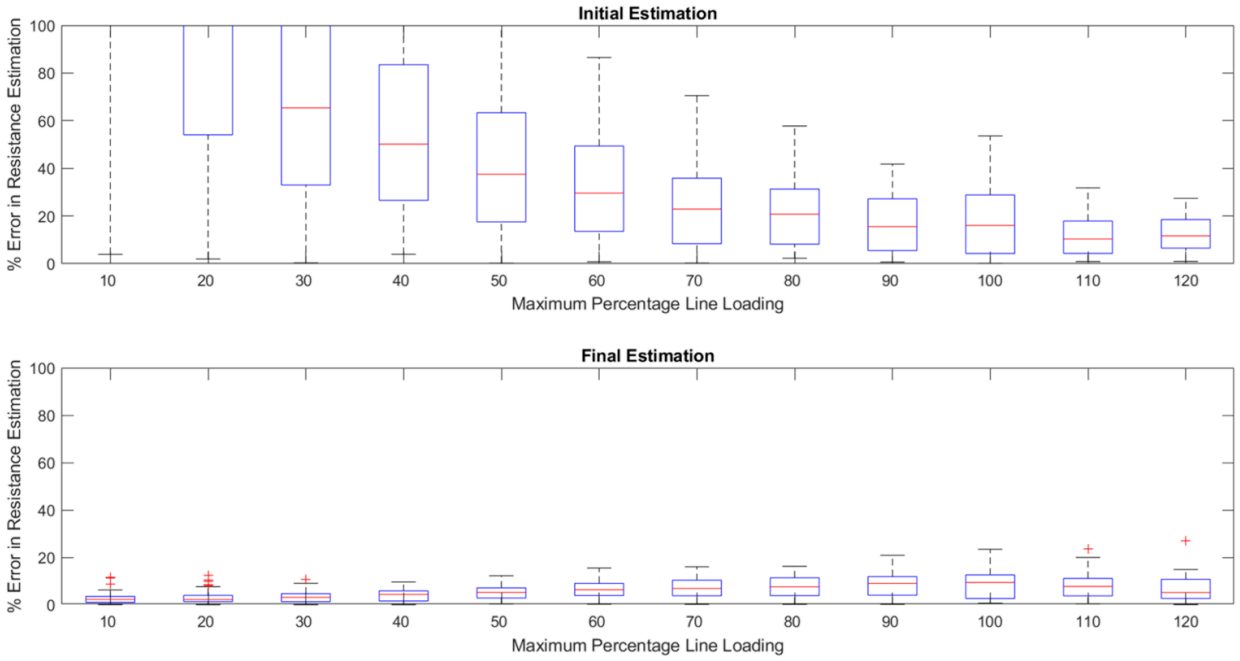

Figure 38. Box plot for error comparison, short line 1.

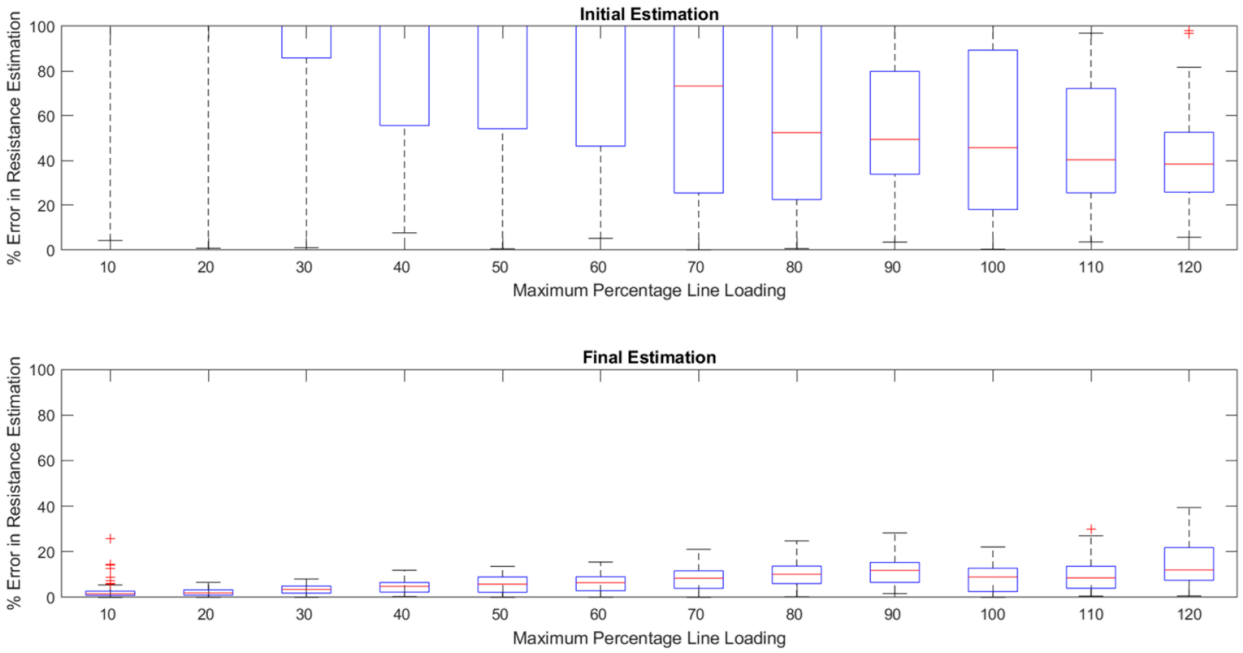

Figure 39. Box plot for error comparison, short line 2.

5.2 Testing on Real Data

The completed algorithm was also tested with continuous real PMU data. As mentioned earlier, the actual resistance of the system is unknown. Yet, since the tests showcased below consist of low line loading conditions, 9.9% and 25% respectively, the expectation is the actual system resistance should be close to or just below the construction model.

In Figure 40 the initial resistance estimation is well beyond the reasonable range. However, the proposed algorithm is able to correct this and outputs a resistance estimation close to the construction value. Since the construction value for this short line assumes a line loading of 70%, the slightly lower final resistance estimations are consistent with the low loading conditions.

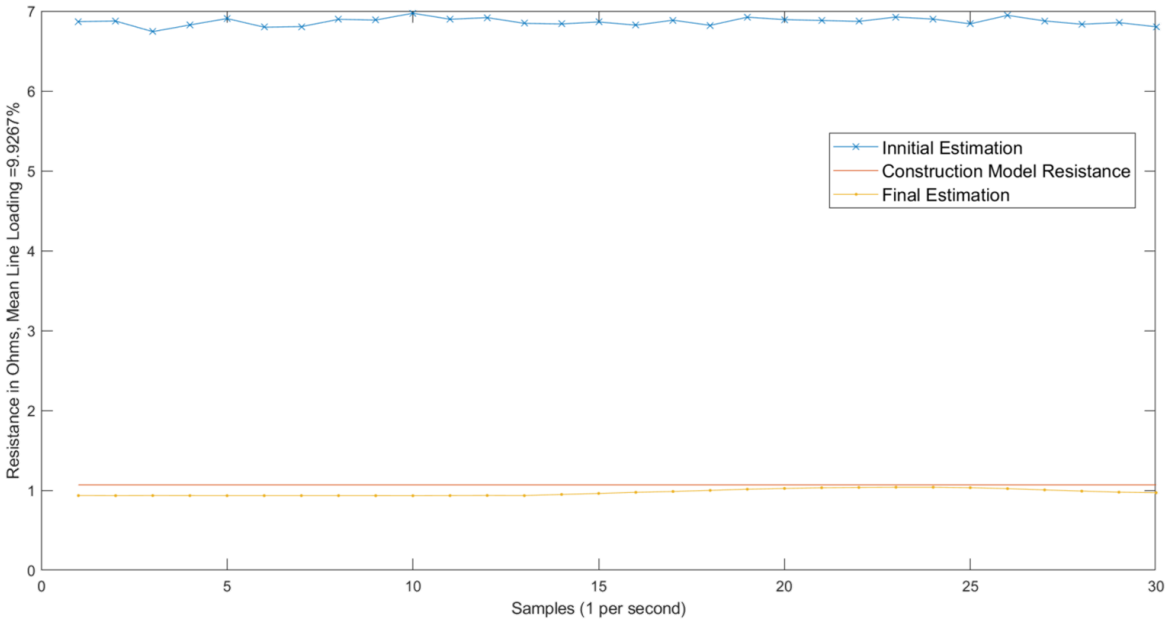

Figure 40. Application on real data, short line.

Figure 41 shows a similar situation on a medium line. Again, the initial resistance estimation is well beyond the reasonable range as expected due to the low loading conditions. The proposed algorithm meanwhile produces acceptable outputs.

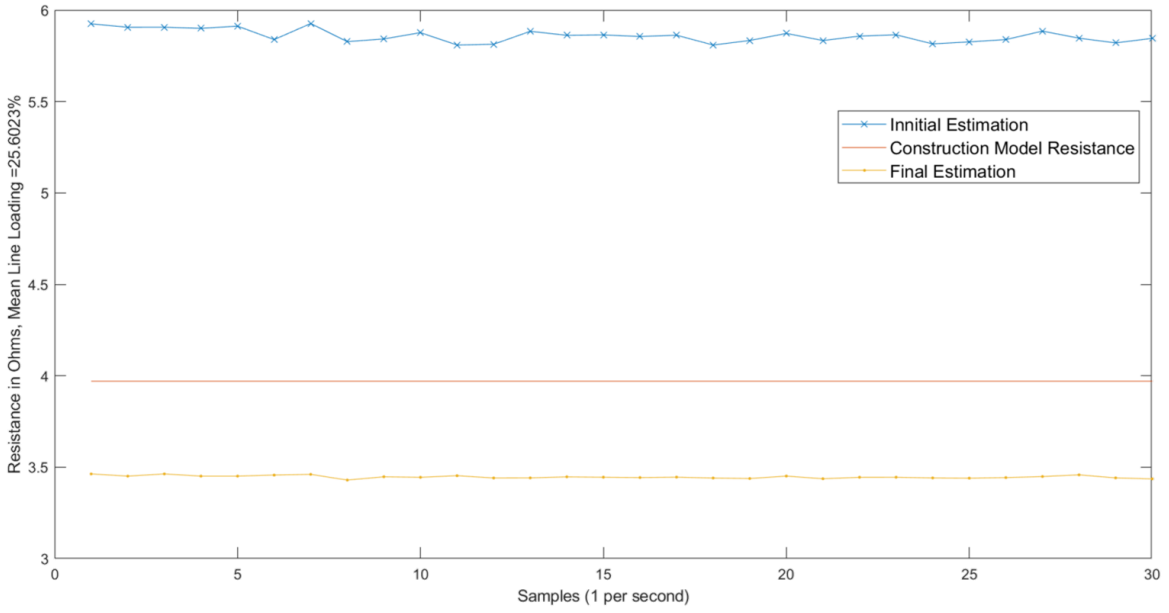

Figure 41. Application on real data, medium line.

Figure 42 shows several cases of resistance estimation from time series PMU data. In all cases, the final resistance estimation is at a more sensible level and consistent with expectations.

- Row 1 and 3 represents periods of high current. Generally, these are the best-case scenarios for the direct estimation method. However, as can be seen in the plot, incorrect estimations, either too high or too low, are possible. The proposed algorithm is able to correct these to a more reasonable value.
- Row 2 and 4 represents periods of low current. These are considered the worst-case scenarios for the direct estimation method and therefore the correction is equally drastic.

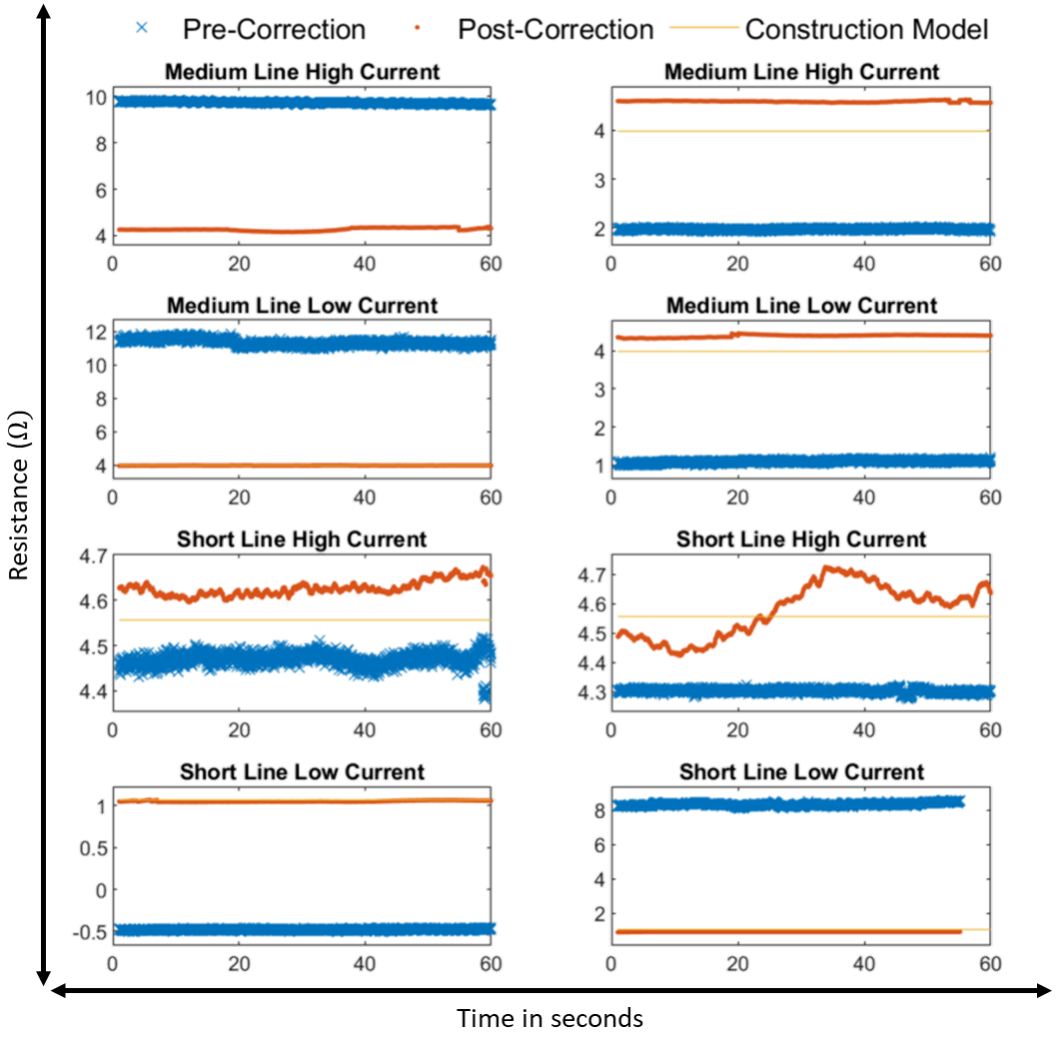

Figure 42. Correction of resistance estimation on real data.

CHAPTER 6

CONCLUSIONS AND FUTURE WORK

6.1 Conclusions

The goal of this work was to create a correction algorithm that could be applied to existing PMU data streams in order to obtain more accurate and usable line resistance estimations. The work was based on an investigation into the fundamental cause of error in PMU data that makes direct resistance estimations unusable. The biasness encountered was proved to be as a result of the allowed error in measurement as per the IEEE standard governing the operation PMUs, defined as Total Vector Error (TVE). This TVE allowance, while not posing a significant issue with the use of single streams of data, would cause the output from calculations involving multiple PMU measured phasor parameters to be unusable in most cases.

In the case of line resistance estimations, the direct estimation method would produce massive errors in all but a very narrow range of high current flow scenarios. A hybrid physics aware learning-based transmission line resistance estimation algorithm is developed to minimize this error based such that the final resistance estimates obtained would be useful to utilities in a range of addiotnal applications, most notable, dynamic line rating estimations.

The algorithm consists of 2 parts. First, a physics-based theory, founded upon research on the effect of TVE, is used to minimize the error in the initial resistance estimations with the use of additional system parameters also obtained from the PMU. A recursive decoupled minimization method is used to deal with the complex nature of the phasor measurements involved. The error minimization method produces corrected resistance estimations that contain significantly less error in comparison to the direct estimations. However, a further step is taken to minimize the error even further.

The error still present in the corrected resistance estimations show distant colorations and relations to several measured system parameters. Therefore, to effectively incorporate the multiple influencing parameters, an artificial neural network based learning algorithm is incorporated. This creates a correction model, unique for each transmission line, that is able to further correct the resistance estimations. The final estimations produced contain minimal error across nearly all current flow regions as shown in the numerical analysis section. The ANN model for each line is easy to create based on accurate simulations and only needs adjustments if physical changes are made to the lines. Since, the proposed estimation algorithm is application in real time, matching the sampling rate of the PMU data, or at a lower sampling rate, based upon needs.

Based on the guidelines proposed, the following are the primary deliverables of this work.

- **Investigate the presence of error in resistance calculation done using real PMU data**. Real PMU data from a utility was used to observe an intrinsic error existing in the measurements. It was observed that the error is amplified when a multiple of these measured values are used in calculations to obtain additional system parameters, most notably in this case, transmission line resistance. It was also observed that the error is vastly more prevalent in low line loading conditions.
- **Develop a hypothesis for the introduction of this error.** An investigation of literature and standards revealed that the Total Vector Error, or the permissible error in measurement, was the prime suspect. Although the set error limits make the data perfectly suitable for use on its own, the compounding of these errors when multiple measurements are used together make the output unusable. The effect of TVE on the interaction between vectors was mathematically simulated and the resulting output matched the observations made on the PMU data based calculations.

- **Recreate this error on synthetic data and compare to that of real data**. A transmission line model was simulated that could accurately recreate artificial PMU measurements with TVE included. This allowed for further investigations into how TVE plays a major role in biased error observed from resistance estimations. The simulation used real system parameters and loads to accurately recreate known transmission lines. The resistance output and the observable error matched very closely to the observations made on real PMU data. The simulated system was also the basis for the creation of the Artificial Neural Network models and their training.
- **Use a fundamental understanding for the cause of this error to develop a correction algorithm for line resistance estimations**. Investigations revealed that due to the sustained biasness in the error observed, statistical correction methods would not yield sufficient improvements. This notion was also prevalent in literature where developed algorithms would perform well on artificial data with unbiased errors but would struggle on real data. Thus, a minimization algorithm was developed to minimize error using knowledge from additional parameters obtained from the PMU data itself. This allowed the bias error to be identified and corrected for. While the resulting corrected estimations showed a vast improvement over direct estimations, the output still lacked the accuracy to be useful to utilities.
- **Use line resistance correlation to environmental factors to further enhance corrected resistance estimates**. External factors such as ambient temperature and wind, while relevant, were difficult to incorporate into a correction model as they could vary significantly over long transmission line spans and would therefore not be a robust approach. However, a study of the corrected resistance estimations and the resulting

correction factors showed that distinct links and correlations exist between these and additional system parameters. To capitalize on this connection, an Artificial Neural Network approach was taken to produce further correction factors that would reduce the remaining error. The resulting ANN model used multiple system parameters, all easily available from the PMU data itself, to produce satisfactory correction factors. The resulting final resistance estimations showed minimal error well within the usability range.

- **Apply the correction algorithm in continuous time format and make use of the correlation to lagged values to further enhance the correction as well as to account for missing data and outliers**. The developed correction algorithm was also applied in continuous time. However, the resulting outputs proved to be accurate enough to not warrant the need for the use of additional lagged values. The lack of lagged values would reduce the burden on the processing requirements as well as allow the algorithm to react to instantaneous changes in the system without delay. A significant issue with missing data and outliers was not found in the data and was therefore not addressed in this work and, instead, would be left as future work.

6.2 Future Work

The To further enhance the usefulness of the methods developed in this work, a number of recommended extensions to this work could be made.

- Develop an outlier detection algorithm and a robust method of data recreation for short spans of missing or unusable data. This would prevent the correction method from making incorrect estimations based off of bad data and would allow the system to continue operating in the presence of short data gaps.

- While dynamic line resistance estimations are valuable for a utility for a number of applications, the most notable of these would be enabling the use of real time PMU data for DLR estimations. Availability of DLR over the whole network would allow utilities to make the most efficient use of the line capacities under favorable conditions.
- The use of resistance estimation to estimate conductor temperature brings with it a number of challenges. This includes the non-homogeneous heating of the conductor due to very local environmental factors [65]. However, this concept could be applied to make conductor temperature estimations over short, critical, spans of the line where the environmental effects could be measured.
- The work could also be extended to estimate line sag and obstacle clearance over short spans of transmission line.

REFERENCES

REFERENCES

[1] "U.S. Energy Information Administration," [Online]. Available: www.eia.gov. [Accessed 15 04 2021].

[2] S. Uski-Joutsenvuo and R. Pasonen , "Maximising power line transmission capability by employing dynamic line ratings – technical survey and applicability in Finland," VTT Technical Research Centre of Finland, 2013.

[3] S. Aivaliotis, "Dynamic Line Ratings for Optimal and Reliable Power Flow," in *FERC Technical Conference*, 2010.

[4] C. S. Engineers, Electrical Transmission and Distribution Reference Book, East Pittsburgh: Westinghouse Electric Corporation, 1964.

[5] Y. Du and Y. Liao, "Online Estimation of Power Transmission Line," in *North American Power Symposium (NAPS)*, Boston, MA, 2011.

[6] M. Asprou and E. Kyriakides, "Identification and Estimation of Erroneous Transmission Line Parameters Using PMU Measurements," *IEEE Transactions on Power Delivery,* vol. 32, no. 6, pp. 2510-2519, 2019.

[7] A. White and S. Jacobs, "Use of Synchrophasors at OG&E".

[8] "IEEE Standard for Synchrophasor Measurements for Power Systems," *IEEE Std C37.118.1a-2014,* 2014.

[9] A. G. Phadke , J. S. Thorp and M. G. Adamiak, "A New Measurement Technique for Tracking Voltage Phasors, Local System Frequency, and Rate of Change of Frequency," *IEEE Transactions on Power Apparatus and Systems,* vol. 102, no. 5, pp. 1025-1038, 1983.

[10] P. Bonanomi, "Phase Angle Measurements with Synchronized Clocks-Principle and Applications," *IEEE Transactions on Power Apparatus and Systems,* vol. 100, no. 12, pp. 5036-5043, 1981.

[11] G. Missout, "Measurement of Bus Voltage Angle Between Montreal and SEPT-ILES," *IEEE Transactions on Power Apparatus and Systems,* vol. 99, no. 2, pp. 536-539, 1980.

[12] G. Missout, J. Beland and G. Bedard, "Dynamic Measurement of the Absolute Voltage Angle on Long Transmission Lines," *IEEE Transactions on Power Apparatus and Systems,* vol. 100, no. 11, pp. 4428-4434, 1981.

[13] A. G. Phadke and J. S. Thorp, Synchronized Phasir Measurements and Their Applications, New York: Springer Science+Business Media, LLC, 2008.

[14] "IEEE/IEC International Standard - Measuring relays and protection equipment - Part 118-1: Synchrophasor for power systems - Measurements," *IEC/IEEE 60255-118-1:2018,* pp. 1-78, 2018.

[15] D. o. Energy, "Smart Grid Investment Grant Program Final Report," 2016.

[16] J. Aghaei, A. Baharvandi, A. Rabiee and M. Akbari, "Probabilistic PMU Placement in Electric Power Networks: An MILP-Based Multiobjective Model," *IEEE Transactions on Industrial Informatics,* vol. 11, no. 2, pp. 332-341, 2015.

[17] F. Aminifar, M. Fotuhi-Firuzabad and A. Safdarian, "Optimal PMU Placement Based on Probabilistic Cost/Benefit Analysis," *IEEE Transactions on Power Systems,* vol. 28, no. 1, pp. 566-567, 2013.

[18] X. Zhu, M. H. F. Wen, V. O. K. Li and K. Leung, "Optimal PMU-Communication Link Placement for Smart Grid Wide-Area Measurement Systems," *IEEE Transactions on Smart Grid,* vol. 10, no. 4, pp. 4446-4456, 2019.

[19] J. S. Thorp, A. G. Phadke, S. H. Horowitz and M. M. Begovic, "Some applications of phasor measurements to adaptive protection," *IEEE Transactions on Power Systems,* vol. 3, no. 2, pp. 791-798, 1988.

[20] M. J. B. Reddy, D. V. Rajesh, P. Gopakumar and D. K. Mohanta, "Smart Fault Location for Smart Grid Operation Using RTUs and Computational Intelligence Techniques," *IEEE Systems Journal,* vol. 8, no. 4, pp. 1260-1271, 2014.

[21] U. Annakkage,, A. Mehrizi-Sani, A. Rajapakse, C. Hauser, B. Bhargava, D. Wadduwage and N. Chaudhuri, "Application of Phasor Measurement Units for Monitoring of Power System Dynamic Performance," International Council on Large Electric Systems, 2017.

[22] V. Aravinthan et al., "Reliability modeling considerations for emerging cyber-physical power systems," in *IEEE International Conference on Probabilistic Methods Applied to Power Systems (PMAPS)*, Boise, ID, 2018.

[23] A. Hettiarachchige-Don et al., "Assessment of System Reliability in Presence of Cyber Attack Risk on PMU Data," in *IEEE International Conference on Information and Automation for Sustainability (ICIAfS)*, Colombo, 2018.

[24] X. Wang, D. Shi, J. Wang, Z. Yu and Z. Wang, "Online Identification and Data Recovery for PMU Data Manipulation Attack," *IEEE Transactions on Smart Grid,* vol. 10, no. 6, pp. 5889-5898, 2019.

[25] A. K. Srivastava, "Phasor Measurement (Estimation) Units," Washington State University, Pullman, WA, 2014.

[26] E. M. Stewart, S. Kiliccote, C. McParland and C. Roberts, "Using Micro-Synchrophasor Data for Advanced Distribution Grid Planning and Operations Analysis," Ernest Orlando Lawrence Berkeley National Laboratory, Berkeley, CA, 2014.

[27] "IEEE Standard for Synchrophasor Data Transfer for Power Systems," 2011.

[28] "Real-Time Application of Synchrophasors for Improving Reliability," North American Electric Reliability Corporation, Princeton, NJ, 2010.

[29] O. Alsac, N. Vempati, B. Stott and A. Monticelli, "Generalized state estimation [power systems]," in *International Conference on Power Industry Computer Applications* , Columbus, OH, 1997.

[30] C. Borda, A. Olarte and H. Diaz, "PMU-based Line and Transformer Parameter Estimation," in *Power Systems Conference and Exposition*, Seattle, WA, 2009.

[31] G. Valverde, D. Cai, J. Fitch and V. Terzija, "Enhanced State Estimation with Real-time Updated Network Parameters Using SMT," in *Power & Energy Society General Meeting*, Calgary, AB, 2009.

[32] R. Baltensperger, A. Loosli, H. Sauvain, M. Zima, G. Andersson and R. Nuqui, "An implementation of two-stage hybrid state estimation with limited number of PMU," in *International Conference on Developments in Power System Protection* , Manchester, 2010.

[33] J. Zhao et al., "Power System Real-Time Monitoring by Using PMU-Based Robust State Estimation Method," *IEEE Transactions on Smart Grid,* vol. 7, no. 1, pp. 300-309, 2016.

[34] R. Matica, V. Kirincic, S. Skok and A. Marusic, "Transmission line impedance estimation based on PMU measurements," in *EUROCON*, Zagreb, 2013.

[35] R. Rubesa, V. Kirincic and S. Skok, "Transmission line positive sequence impedance estimation based on multiple scans of Phasor Measurements," in *IEEE International Energy Conference*, Cavtat, 2014.

[36] D. L. Alvarez, J. A. Rosero, F. Faria da Silva, C. L. Bak and E. E. Mombello, "Dynamic line rating — Technologies and challenges of PMU on overhead lines: A survey," in *51st International Universities Power Engineering Conference (UPEC)*, Coimbra, 2016.

[37] J. Lehman, "Line Impedance Estimation Project," Idaho Power, 2015.

[38] D. Shi, D. J. Tylavsky and N. Logic, "An Adaptive Method for Detection and Correction of Errors in PMU Measurements," *IEEE Transactions on Smart Grid,* vol. 3, no. 4, pp. 1575-1583, 2012.

[39] C. Pisani, A. Vaccaro and D. Villacci, "Conceptualization and Experimental Deployment of an Adaptive Synchronized Sensing System for Power Line Thermal Monitoring," *IEEE Transactions on Industrial Informatics,* vol. 12, no. 6, pp. 2158-2165, 2016.

[40] A. M. Prostejovsky, O. Gehrke, A. M. Kosek, T. Strasser and H. W. Bindner, "Distribution Line Parameter Estimation Under Consideration of Measurement Tolerances," *IEEE ransactions on Industrial Informatics,* vol. 12, no. 2, pp. 726-735, 2016.

[41] S. Wang, J. Zhao, Z. Huang and R. Diao, "Assessing Gaussian Assumption of PMU Measurement Error Using Field Data," *IEEE Transactions on Power Delivery,* vol. 33, no. 6, pp. 3233-3236, 2018.

[42] D. Ritzmann, P. S. Wright, W. Holderbaum and B. Potter, "A Method for Accurate Transmission Line Impedance Parameter Estimation," *IEEE Transactions on Instrumentation and Measurement,* vol. 65, no. 10, pp. 2204-2213, 2016.

[43] G. Sivanagaraju, S. Chakrabarti and S. C. Srivastava, "Uncertainty in Transmission Line Parameters: Estimation and Impact on Line Current Differential Protection," *IEEE Transactions on Instrumentation and Measurement,* vol. 63, no. 6, pp. 1496-1504, 2014.

[44] F. Ding, C. D. Booth and A. J. Roscoe, "Peak-Ratio Analysis Method for Enhancement of LOM Protection Using M-Class PMUs," *IEEE Transactions on Smart Grid,* vol. 7, no. 1, pp. 291-299, 2016.

[45] X. Wang, H. Sun, B. Zhang, W. Wu and Q. Guo, "Real-time local voltage stability monitoring based on PMU and recursive least square method with variable forgetting factors," in *IEEE Innovative Smart Grid Technologies - Asia (ISGT Asia)*, Tianjin, 2012.

[46] H. Su and C. Liu, "Estimating the Voltage Stability Margin Using PMU Measurements," *IEEE Transactions on Power Systems,* vol. 31, no. 4, pp. 3221-3229, 2016.

[47] H. Su and C. Liu, "An Adaptive PMU-Based Secondary Voltage Control Scheme," *IEEE Transactions on Smart Grid,* vol. 4, no. 3, pp. 1514-1522, 2013.

[48] L. Huang, Y. Sun, J. Xu, W. Gao, J. Zhang and Z. Wu, "Optimal PMU Placement Considering Controlled Islanding of Power System," *IEEE Transactions on Power Systems,* vol. 29, no. 2, pp. 742-755, 2014.

[49] Q. Jiang, B. Wang and X. Li, "An Efficient PMU-Based Fault-Location Technique for Multiterminal Transmission Lines," *IEEE Transactions on Power Delivery,* vol. 29, no. 4, pp. 1675-1682, 2014.

[50] Joe-Air Jiang, Jun-Zhe Yang, Ying-Hong Lin, Chih-Wen Liu and Jih-Chen Ma, "An adaptive PMU based fault detection/location technique for transmission lines. I. Theory and algorithms," *IEEE Transactions on Power Delivery,* vol. 15, no. 2, pp. 486-493, 2000.

[51] R. S. Singh, S. Cobben, M. Gibescu, H. van den Brom, D. Colangelo and G. Rietveld, "Medium Voltage Line Parameter Estimation Using Synchrophasor Data: A Step Towards Dynamic Line Rating," in *IEEE Power & Energy Society General Meeting (PESGM)*, Portland, OR, 2018.

[52] D. L. Alvarez, F. da Silva, E. Mombello, C. Bak and J. Rosero, "Conductor Temperature Estimation and Prediction at Thermal Transient State in Dynamic Line Rating Application," *IEEE Transactions on Power Delivery,* vol. 33, no. 5, pp. 2236-2245, 2018.

[53] L. Dawson and A. Knight, "Applicability of Dynamic Thermal Line Rating for Long Lines," *IEEE Transactions on Power Delivery,* vol. 33, no. 2, pp. 719-727, 2018.

[54] M. K. Hasan et al. , "An Improved Dynamic Thermal Current Rating Model for PMU-Based Wide Area Measurement Framework for Reliability Analysis Utilizing Sensor Cloud System," *Special Section on Reliabilty in Sensor-Cloud System and Applications,* vol. 9, pp. 14446-14458, 2021.

[55] D. Gurusinghe and A. D. Rajapakse, "Efficient Algorithms for Real-Time Monitoring of Transmission Line Parameters and Their Performance with Practical Synchrophasors," *IET Generation Transmission & Distribution,* vol. 11, pp. 1134-1143, 2017.

[56] A. Riepnieks and H. Kirkham, "An Introduction to Goodness of Fit for PMU Parameter Estimation," *IEEE Transactions on Power Delivery,* vol. 32, no. 5, pp. 2238-2245, 2017.

[57] J. D. Glover, M. S. Sarma and T. Overbye, Power System Analysis and Design, Brooks/Cole Publishing Co., 2012.

[58] S. M. Westervelt, "Transmission Line Positive Sequence Parameter Determination using Synchronized Phasor Measurement," Wichita State University, Wichita, KS, 2015.

[59] D. Gurusinghe, "Application of Wide Area Synchrophasor Measurements for Improved Real-Time Monitoring and Control of Power Systems," University of Manitoba, Winnipeg,, 2016.

[60] D. Shi, D. J. Tylavsky, N. Logic and K. M. Koellner, "Identification of Short Transmission-Line Parameters from Synchrophasor Measurements," in *North American Power Symposium*, Calgary, AB, 2008.

[61] Y. X. S. Zhang, "Solving Nonlinear Optimization Problems of Real Functions in Complex Variables by Complex-Valued Iterative Methods," *IEEE Transactions on Cybernetics,* vol. 48, no. 1, pp. 277-287, 2018.

[62] A. Back, Theory, Algorithms, and Applications with MATLAB, Philadelphia, PA: Mathematical Optimization Society and the Society for Industrial and Applied Mathematics, 2014.

[63] R. Baldick, Applied Optimization, Formulation and Algorithms for Engineering Systems, Cambridge: Cambridge University Press, 2008.

[64] K. Levenberg, "A Method for the Simulation of Certain Non-Linear Problems in Least Squares," in *Annual Meeting of the American Mathematical Society*, Chicago, 1943.

[65] D. Alvarez, J. Rosero, F. Faria da Silva, C. Bak and E. Mombello, "Dynamic line rating — Technologies and challenges of PMU on overhead lines: A survey," in *51st International Universities Power Engineering Conference (UPEC)*, Coimbra, 2016.

[66] C. P. Steinmetz, "Complex quantities and their use in electrical engineering," in *Proceedings of the International Electrical Congress*, Chicago, 1893.

APPENDICES

APPENDIX A

MATHAMATICAL REPRESENTATION OF PHASORS

In 1893, Charles Proteus Steinmetz published his findings on using complex mathematical techniques to model AC networks for analysis [66]. Using these findings and facilitated by the ever advancing processing power available, researchers developed various techniques for the real time monitoring of transmission lines. In 1983,

The mathematical representation of an AC waveform in time domain can be in the form of equation,

$$x(t) = X_m \,\mathrm{COS}(\omega t + \theta)$$

Where X_m is the magnitude of the sinusoidal waveform and θ is the angular reference of the waveform. ω is from the equation $\omega = 2 \times \pi \times f$, where f is the instantaneous frequency. In phasor form, this equation would be represented as shown.

$$\bar{X} = X_m \angle \theta$$

If the value is in RMS, as in equation below would represent the phasor.

$$\bar{X}_{rms} = \frac{X_m}{\sqrt{2}} \angle \theta$$

The correlation between the domains of the equations can be represented as shown in Figure 43. Plot (a) shows the function in time domain while plot (b) graphs the function as a phasor.

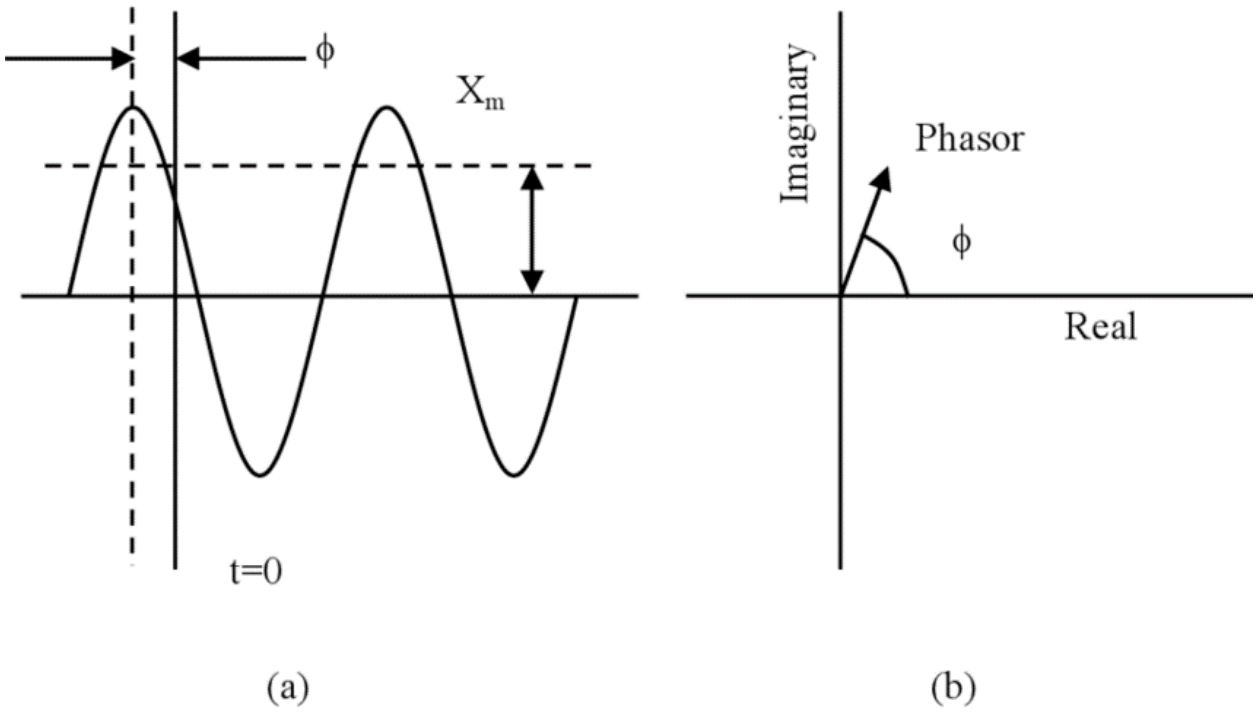

Figure 43. Correlation between time domain and a phasor representation [13].

APPENDIX B

PMU PARAMETERS TRANSMITTED (SINGLE-PHASE)

Parameters and measurements contained in each PMU record in single-phase PMU data.

Data Field	**Parameter**
TimeStamp	Precise GPS time tag.
TermID	Unique Identifier for the PMU
CurrentMag	RMS Current Magnitude
CurrentAng	Phasor Angle for Current
VoltageMag	RMS Voltage Magnitude
VoltageAng	Phasor Angle for Voltage
Frequency	Instantaneous Frequency
DFDT	Rate of Change of Frequency
Status	Circuit Switching Status
Digitals	Digital Relay Information

APPENDIX C

PMU PARAMETERS TRANSMITTED (THREE-PHASE)

Parameters and measurements contained in each PMU record in three-phase PMU data.

Data Field	**Parameter**
TimeStamp	Precise GPS time tag.
TermID	Unique Identifier for the PMU
Terminal	PMU location (Substation 1 to Substation 2)
V_M_A	RMS Voltage Magnitude in Phase A
V_A_A	Phasor Angle for Voltage in Phase A
I_M_A	RMS Current Magnitude in Phase A
I_A_A	Phasor Angle for Current in Phase A
V_M_B	RMS Voltage Magnitude in Phase B
V_A_B	Phasor Angle for Voltage in Phase B
I_M_B	RMS Current Magnitude in Phase B
I_A_B	Phasor Angle for Current in Phase B
V_M_C	RMS Voltage Magnitude in Phase C
V_A_C	Phasor Angle for Voltage in Phase C
I_M_C	RMS Current Magnitude in Phase C
I_A_C	Phasor Angle for Current in Phase C
V_M_1	RMS Voltage Magnitude in positive sequence
V_A_1	Phasor Angle for Voltage in positive sequence
I_M_1	RMS Current Magnitude in positive sequence
I_A_1	Phasor Angle for Current in positive sequence
Frequency	Instantaneous Frequency
DFDT	Rate of Change of Frequency
Status	Circuit Switching Status
Digitals	Digital Relay Information